ADVANCED STRUCTURAL CHARACTERISATION OF AGAR-BASED HYDROGELS: RHEOLOGICAL AND SMALL ANGLE SCATTERING STUDIES

Marta Martínez-Sanz[1*], Anna Ström[2], Patricia Lopez-Sanchez[3], Svein Halvor Knutsen[4], Simon Ballance[4], Hanne Kristine Zobel[4], Anna Sokolova[5], Elliot Paul Gilbert[5,6] and Amparo López-Rubio[1]

[1]Food Safety and Preservation Department, IATA-CSIC, Avda. Agustin Escardino 7, 46980 Paterna, Valencia, Spain

[2]Dept. Chemistry and Chemical Engineering, Chalmers University of Technology, Gothenburg, Sweden.

[3]Agrifood and Bioscience, RISE Research Institutes, SE 41273 Gothenburg, Sweden

[4]Nofima AS, Norwegian Institute of Food, Fisheries and Aquaculture Research, Ås, Norway

[5]Australian Centre for Neutron Scattering, Australian Nuclear Science and Technology Organisation, Locked Bag 2001, Kirrawee DC, NSW 2232, Australia

[6] The Australian Institute for Bioengineering and Nanotechnology and Queensland Alliance for Agriculture and Food Innovation, The University of Queensland, Brisbane, QLD 4072, Australia

*Corresponding author: Tel.: +34 963200022; fax: +34 963636301

E-mail address: mmartinez@iata.csic.es

Graphical Abstract

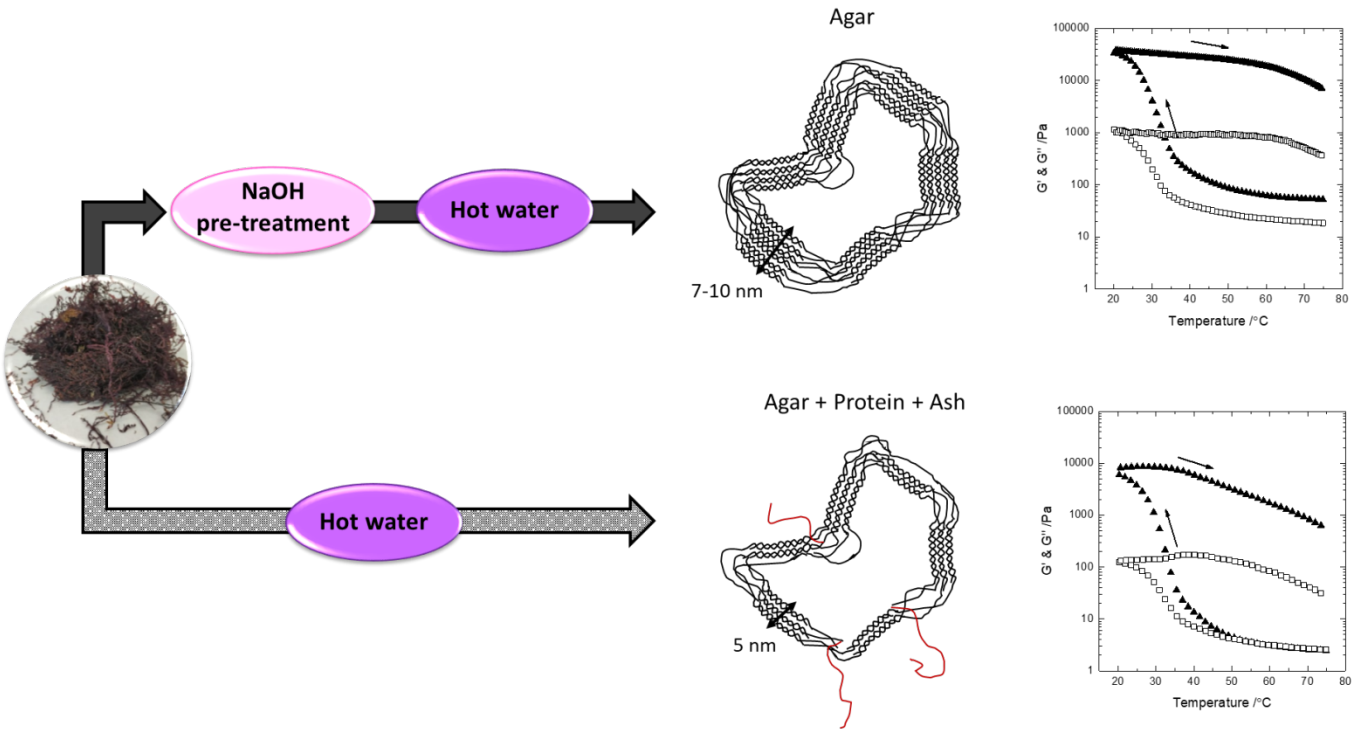

Abstract

Agar-based extracts from *Gelidium sesquipedale* were generated by heat and combined heat-sonication, with and without the application of alkali pre-treatment. Pre-treatment yielded extracts with greater agar contents; however, it produced partial degradation of the agar, reducing its molecular weight. Sonication produced extracts with lower agar contents and decreased molecular weights. A gelation mechanism is proposed based on the rheological and small angle scattering characterization of the extracts. The formation of strong hydrogels upon cooling was caused by the association of agarose chains into double helices and bundles, the sizes of which depended on the agar purity and molecular weight. These different arrangements at the molecular scale consequently affected the mechanical performance of the obtained hydrogels. Heating of the hydrogels produced a gradual disruption of the bundles; weaker or smaller bundles were formed upon subsequent cooling, suggesting that the process was not completely reversible.

Keywords: seaweed; *Gelidium sesquipedale*; rheology**;** SAXS; SANS; molecular weight

1. Introduction

Agar is a mixture of polysaccharides which represent the main structural components in the cell walls from several seaweeds (such as *Gelidium* and *Gracilaria*) of the Rhodophyceae (red algae) class. This material is widely used within the food industry and microbiology fields due to its excellent gelling properties, i.e. it forms gels with relatively high thermal stability and gel strength. Agarose is the idealized structure of agar (Araki, 1966), which consists of repeating units of agarobiose or $(LA\text{-}G)_n$ (Knutsen, Myslabodski, Larsen, & Usov, 1994); alternating β-D-galactopyranosyl and 3,6-anhydro-α-L-galactopyranosyl groups. However, this backbone is in general masked by substituent groups such as sulphate esters, methyl ethers or pyruvate acid ketals (Duckworth & Yaphe, 1971), which most often reduce the gelling ability and influence gelling temperature and melting behaviour. The native seaweed source and the protocol used for the extraction are determinant factors for the occurrence of the substituent groups in the agar structure and have a strong impact on the physicochemical, mechanical and rheological properties of the extracted agar (Freile-Pelegrín & Robledo, 1997; Sousa, Borges, Silva, & Gonçalves, 2013). Alkaline treatments, which are routinely applied in the agar manufacturing process, convert L-galactose-6-sulphate units into 3,6-anhydro-L-galactose which, in turn, improve the purity and mechanical properties of agar gels (Armisen & Galatas, 1987). Nevertheless, the application of these alkaline pre-treatments may result in partial degradation and loss of the agar during washing and produce significantly lower final extraction yields (Lee et al., 2017; Meena, Prasad, Ganesan, & Siddhanta, 2007). Alternative extraction protocols based on heating treatments, as well as their combination with sonication, have been recently explored for the production of less purified agar-based extracts with the aim of optimizing industrial processes in terms of time and energy consumption (Martínez-Sanz, Gómez-Mascaraque, et al., 2019). These agar-based extracts were reported to form softer gels with

87 antioxidant capacity, which may be interesting for a wide range of alternative applications
88 such as food additives, food packaging structures (Martínez-Sanz, Martínez-Abad, &
89 López-Rubio, 2019) and encapsulation of bioactive components (Alehosseini et al., 2018).
90
91 Despite the great scientific and industrial interests in agar, the mechanism driving the
92 gelation process and the specific role of different components are still not fully understood.
93 The formation of gels has been hypothesized to occur through a sequential two-step process.
94 The first step consists of the transition from a random coil conformation in solution at high
95 temperatures (around 95 ºC) to a rigid, ordered structure of double helices upon cooling
96 (Arnott et al., 1974). These helices are thought to provide the junction zones necessary for
97 the gel network formation (Mohammed, Hember, Richardson, & Morris, 1998). Upon
98 further cooling, the helices aggregate to form thick bundles, resulting in the formation of
99 strong gels. Although the formation of double helices seems to be crucial in the gelation
100 process, their aggregation into bundles appears to be principally responsible for the
101 formation of stable and strong gels (Dai & Matsukawa, 2012). In fact, one peculiarity of
102 agar gels is their large thermal hysteresis, i.e. the reported melting temperatures ($T_m \approx$ 80-
103 95 °C) are typically much higher than the gelling temperatures ($T_g \approx$ 28-47 °C) (Lahrech,
104 Safouane, & Peyrellasse, 2005; Medina-Esquivel, Freile-Pelegrin, Quintana-Owen, Yáñez-
105 Limón, & Alvarado-Gil, 2008). This phenomenon has been attributed to the high stability
106 of the agarose bundles, which are disrupted at temperatures much higher than those at which
107 they are formed upon cooling (Indovina, Tettamanti, Micciancio-Giammarinaro, & Palma,
108 1979). It is not fully understood how the formation of double helices and bundles is affected
109 by the occurrence of agar substituents and much less, by the presence of other components
110 such as proteins, which may interact with agar. Thus, further studies are required to
111 investigate the impact of different factors (such as agar purity, molecular weight and type

and amount of substituents) on the gelation mechanism of agar and also to enable the rational design of novel extraction protocols based on the agar requirements that depend on its final intended application. For instance, softer gels could be designed for food related applications where high gel strength is not a requirement (thickening agents), using cheaper and simpler extraction protocols. On the other hand, for microbiology applications, where stronger gels with greater degree of purity are required, a pre-treatment step would be required to remove other components present in the raw seaweed.

In this context, small angle X-ray and neutron scattering techniques (SAXS and SANS) offer an advantage to investigate the nanoscale structure of agar gels in their native state since, unlike other methods, minimal sample preparation is required thus avoiding structural alterations in the samples. Furthermore, in the case of SANS, the different scattering length of hydrogen and deuterium enables selective scattering length density modification to generate contrast between diverse components in the samples. The possibility of carrying out temperature-resolved experiments represents an additional opportunity to investigate the structural changes taking place during the sol-gel transition in hydrogels. In fact, the combination of SAXS and SANS with complementary techniques has been proven to be extremely powerful to understand the structure of different polysaccharide-based hydrogels (Gómez-Mascaraque, Llavata-Cabrero, Martínez-Sanz, Fabra, & López-Rubio, 2018; Martínez-Sanz, Mikkelsen, Flanagan, Gidley, & Gilbert, 2016; Yu, Yakubov, Martínez-Sanz, Gilbert, & Stokes, 2018). Despite this, the application of SAXS and SANS to investigate the structure and gelation mechanism of agar has been very limited to date and only a few studies, mostly carried out on pure agarose, are available in the literature (Djabourov, Clark, Rowlands, & Ross-Murphy, 1989; Krueger, Andrews, & Nossal, 1994; Rochas, Hecht, & Geissler, 1999). Moreover, the complexity in

interpreting the scattering data, and difficulties in identifying a suitable structural model, have prevented the full potential of these techniques in being exploited.

In this study, we investigated the nanostructure of hydrogels from agar-based extracts using advanced small angle scattering techniques and rheology. The effect of molecular structure and composition of the extracts generated by different extraction methods on the gelation mechanism was evaluated and related to the mechanical properties of the generated gels.

2. Materials and methods

2.1 Materials

Dried *Gelidium sesquipedale* and the commercial grade agar PRONAGAR (batch reference H-3544/19) were kindly donated by Hispanagar (Burgos, Spain). The dry seaweed was ground into a fine powder before further processing.

2.2 Agar extraction

Agar was extracted from *Gelidium sesquipedale* seaweed by applying heat or combined heat-sonication extraction procedures, as described in a previous work (Martínez-Sanz, Gómez-Mascaraque, et al., 2019). Briefly, 50 g of dry seaweed powder was dispersed in 500 mL of distilled water and heated and held at 90 ºC for 2 h with stirring (heat extraction) or subjected to simultaneous heating at 90 ºC and sonication using an ultrasound probe operating at 400 W and a constant frequency of 24 kHz for 30 min (combined heat-sonication extraction). The hot agar-based solution was separated from the insoluble material by filtration with muslin cloth. The filtrate was allowed to gel at room temperature and frozen overnight. Subsequently, the material was subjected to two freeze-thaw cycles to remove low molecular weight water-soluble molecules and the purified agar-based gel was freeze-

dried. The samples obtained from the heat and the combined heat-sonication extraction protocols were coded as HW and HW-US, respectively. Additionally, the application of a conventional pre-treatment with hot NaOH prior to the extraction process, as described in (Martínez-Sanz, Gómez-Mascaraque, et al., 2019), was also performed for both abovementioned treatments, hence obtaining the samples coded as NaOH+HW and NaOH+HW-US, respectively.

2.3 Compositional analysis of the agar-based extracts

Carbohydrate composition via reductive hydrolysis

A procedure adapted from Quemener and Lahaye (Quemener & Lahaye, 1998) was followed. Typically, 10 mg of sample were dissolved in 5 mL of aqueous myo-inositol (0.5 mg/mL) by heating at 95 °C for 45 min. After cooling to 50 °C, 500 μL aliquots were evaporated to dryness at 50 °C in a stream of nitrogen. A pre-hydrolysis was initiated by adding 50 μL of morpholine borane (MMB) (80 mg/ml) and 200 μL of 3 M trifluoroacetic acid (TFA) and heating at 80 °C for 30 min. After cooling, 50 μL of MMB was added and the solution evaporated to dryness again. The main hydrolysis was then performed by adding 200 μL of 2 M TFA at incubating at 120 °C for 1 h. Samples were then cooled, 100 μL of MMB added, and evaporated to dryness again. After adding 500 μL of acetonitrile, the samples were evaporated to dryness and acetylation was performed according to Stevenson and Furneaux (Stevenson & Furneaux, 1991). Aqueous solutions of standard sugars (galactose, 3,6 anhydro-L-galactose, glucose and xylose), also containing an internal standard (myo-inositol), were treated in the same way to construct standard curves for quantification. Enzymatically produced di- and tetra-saccharides of 4-sulphated neocarrabiose, DA-G4S and $(DA\text{-}G4S)_2$ respectively from kappa-carrageenan $(DA\text{-}G4S)_n$ were included both as a positive control in the GC procedure and for sulphur determination.

Alditol acetates were separated on an SGE BPX 70 capillary column (25 m x 0.22 mm x 0.25 µm) using an Agilent 7890B GC. 1 µL sample was injected and split 40:1 at 250 °C. Column helium flow was set to 3 mL/min, the initial temperature was 200 °C and raised to 220 °C at a rate of 1 °C/min. Flow was split after the column outlet via a deactivated fused silica column to an Agilent 5977B EI-MSD and FID detector with the FID detector temperature set to 250 °C. The MSD transfer line temperature was 300 °C, solvent delay 3 min and data collection 2.9 scans/s. Mass spectra were collected from 44 to 550 m/z. Identification of eluting peaks was made with EI-MS against literature spectra (Bellion, Brigand, Prome, Welti, & Bociek, 1983; Chizhov, Zolotarev, Usov, Rechter, & Kocchetkov, 1971) or NIST mass spectral search program version 2.2. Quantification was made by FID using calibration via the available sugar standards or, where standards were not available, by using relative weight response factors (relative to myo-inositol) computed from published relative molar response (RMRF) factors. For 2-O-Me-3,6 anhydro- galactose (1,4,5-tri-O-acetyl-3,6-anhydro-2-O-methyl galactitol), the RMRF was 0.64 and for 6-O-methylgalactose (1,2,3,4,5-penta-O-acetyl-6-O-methyl galactitol), it was 0.84 (Stevenson & Furneaux, 1991). All data were processed with Agilent Masshunter software. Results are reported as g polysaccharide per 100 g dry weight sample.

Sulphur and nitrogen analysis

Sulphur and nitrogen contents were measured by elemental analysis via total combustion using a Vario-EL-cube elemental analyser. Values for sulphur are reported directly as % of dry weight or as degree of sulphate substitution of the idealized neoagarobiose backbone $(LA\text{-}G)_n$, using the formula DS= 4.5 x (S%/C%) as proposed by Melo et al. (Melo, Feitosa, Freitas, & De Paula, 2002). The measured sulphur content for $(DA\text{-}G4S)_2$ was 7.76 % with

a corresponding calculated DS of 1.00 which correlates to one sulphate group per neocarribiose dimer. Crude protein was estimated by the formula %N x 6.25.

Ash content

Ash content was determined by the standard method TAPPI T211 om-07. Briefly, dry samples (ca. 1 g) were placed in a muffle furnace for at least 4 h at 525 ºC ± 25 ºC. Ash content was measured from the ratio of the resulting material divided by the initial dry weight. Determinations were carried out in duplicate.

2.4 Weight-average molecular weight and intrinsic viscosity

A similar procedure to that reported by Rochas & Lahaye (Rochas & Lahaye, 1989) was followed, except that a low angle light scattering detector (LALLS) was replaced by a multi-angle light scattering detector (MALLS) and an on-line viscometer rather than a capillary Ubbelhode viscometer was used. To 10-20 mg samples, 0.1 M $NaNO_3$ containing 0.02 % NaN_3 was added to make a concentration of 1 mg/mL. Tubes were kept in a boiling water bath for 20-30 min, until tube contents visually dissolved. Aliquots of the samples were then centrifuged while still hot at 13300 rpm in a MICROSTATR 17 bench centrifuge (VWR) for 10 min. 1 mL of supernatant was transferred to new tubes and again left in a boiling water bath for 1-2 min. Samples were then transferred to pre-heated vials and the sample tray kept at 95 °C. 100 µL of the unfiltered sample was injected via an autosampler. The chromatography equipment comprised a Shimadzu LC-20 HPLC system delivering 0.1 M sodium nitrate/0.02% azide at 0.5 mL/min to a guard-column (Tosoh PWXL) and then to two serially-connected size-exclusion columns (TosohTSK-gel G6000 PWXL followed by G5000PWXL) thermostatted at 45 °C in a column oven. The detection system comprised a Dawn Helios +8 eight angle MALLS, a Viscostar II viscometer and an Optilab T-Rex RI

detector (Wyatt, California, USA). Astra version 6 (Wyatt, California, USA) was used to collect and process raw data. The refractive index increment (*dn/dc*) was taken to be 0.140 mL/g and, assuming low solute concentrations, non-ideality effects were to be assumed negligible; the second virial coefficient (A_2) was therefore set to 0.

2.5 Preparation of agar-based dispersions and hydrogels

Dispersions from the agar-based extracts were prepared at a concentration of 1.5% (w/w) in distilled water. To disperse the agar-based extracts, the required amount of freeze-dried sample was added to distilled water and heated to ca. 95 ºC for 45 min. Aliquots of the hot solutions were directly transferred to SAXS capillaries or the rheometer plate. For the compression tests and the SANS experiments, the hot solutions were transferred to methacrylate moulds (18 mm diameter) and were cooled to 25 ºC overnight to obtain disk-like hydrogel specimens.

2.6 Oscillatory rheological measurements

Storage (G') and loss (G'') moduli of the systems were determined using a DHR-3 rheometer from TA Instruments, USA. A cone-and-plate geometry (4 cm diameter, 1º angle and 26 μm of gap) was used in all measurements. Temperature was controlled using a Peltier plate. To avoid evaporation, the cone was equipped with a solvent trap and an evaporation blocker from TA Instruments and the samples were covered with a layer of paraffin oil. The freshly prepared hot agar solutions, kept at 75 ºC until the beginning of the experiments, were added to the rheometer, which was pre-heated at 75 ºC. After an equilibration time of 5 min, a cooling step from 75 ºC to 20 ºC was performed at a constant rate of 1 ºC/min and with a constant strain of 1% and frequency of 6.28 rad/s. The samples were then kept at 20 ºC during 10 min. Finally, a heating step from 20 ºC to 75 ºC was carried out at a rate of 1

ºC/min, 1% strain and a fixed frequency of 6.28 rad/s. Frequency sweeps were also performed at different selected temperatures. The samples, initially equilibrated at 80 ºC, were cooled down to the desired temperature at a rate of 1 ºC/min and frequency sweeps within the range of 0.05-100 rad/s were carried out, at 1% strain amplitude. All measurements were performed at least in duplicate.

2.7 Uniaxial compression

Uniaxial compression tests were performed on an Instron material testing device (model 5542, Instron, Norwood, MA, USA). Gel disk specimens were removed from the moulds and placed between flat metal surfaces covered with emery paper to avoid slippage. A 3 cm cylindrical probe was used to compress the gels until fracture, using a 500 N load cell at a crosshead speed of 0.1 mm/s. At least three replicates of each type gel were measured. Force (N) and distance (mm) were converted to true stress (σ_T) and true strain (ε_T) using equations 1 and 2 by the instrument software Blue Hill.

$$\sigma_T = \frac{F(t)(h_0 - \Delta h(t))}{\pi r_0^2 h_0} \quad (1)$$

$$\varepsilon_T = \ln\left(\frac{h_0}{h_0 - \Delta h(t)}\right) \quad (2)$$

where h_0 is the initial height of the sample, $\Delta h(t)$ is the change in height during compression and r_0 is the initial radius of the sample. Young moduli (E) were obtained as the slope of the initial linear zone of the true stress vs. true strain plots.

2.8 Temperature-resolved small angle X-ray scattering (SAXS) experiments

Small angle X-ray scattering (SAXS) experiments were carried out in the Non Crystalline Diffraction beamline, BL-11, at ALBA synchrotron light source (www.albasynchrotron.es). Aliquots of agar solutions were placed in sealed 2 mm quartz

capillaries (Hilgenburg Gmbh, Germany) and were left to cool to 25 ºC for 24 h to form gels prior to the experiments. The energy of the incident photons was 12.4 keV or equivalently a wavelength, λ, of 1 Å. The SAXS diffraction patterns were collected by means of a Pilatus 1M photon counting detector with an active area of 168.7x 179.4 mm^2, an effective pixel size of 172 x 172 μm^2 and a dynamic range of 20 bits. The sample-to-detector distance was set to 6425 mm, resulting in a q range with a maximum value of q = 0.23 $Å^{-1}$, where q is the magnitude of the scattering vector, defined as $q = \frac{4\pi}{\lambda}\sin\theta$, and 2θ is the scattering angle. An exposure time of 0.5 s was selected based on preliminary trials.

Samples were heated from 25 ºC to 95 ºC at a heating rate of 1 ºC/min, kept at 95 ºC for 30 min and then cooled down from 95 ºC to 10 ºC at a cooling rate of 1 ºC/min. Data were collected in frames of 30 s, followed by a period of 30 s in which the samples were protected from the beam by a local shutter. Each data frame thus corresponds to a temperature range of 1 ºC. The data reduction was treated by pyFAI python code (ESRF) (Kieffer & Wright, 2013), modified by ALBA beamline staff, to perform on-line azimuthal integrations from a previously calibrated file. The calibration files were created from a silver behenate standard. The radially averaged intensity profiles were then represented as a function of q using the IRENA macro suite (Ilavsky & Jemian, 2009) within the Igor software package (Wavemetrics, Lake Oswego, Oregon). A scattering background corresponding to a quartz capillary filled with water was subtracted from all the samples.

2.9 Small angle neutron scattering (SANS)

SANS measurements were performed on the BILBY (Sokolova et al., 2019) instrument at the Australian Centre for Neutron Scattering, ANSTO with a range of neutron wavelengths from 2 to 18 Å. The rear detector was placed at 10 m and the sample-to-detector distance

to the top/bottom and left/right curtains were 4.0 m and 3.0 m respectively; the left and right curtain opening was 350 mm, and that of the top and bottom curtains was 200 mm. This set-up enables to coverage in q from 0.0023 to 0.98 $Å^{-1}$. Pre-formed agar-based hydrogels were placed in 2 mm path length cells with demountable quartz windows and the cells were filled with the required solvent (H_2O, D_2O or different H_2O/D_2O mixtures). To maximize D/H exchange, prior to the SANS measurements, the hydrogels were initially soaked for 24 h in 50 mL of D_2O or H_2O/D_2O mixtures and, subsequently, an additional exchange step with fresh solvent was carried out for at least a further 24 h. Note that this is in vast excess with respect to the polymer. Data reduction followed BILBY-specific procedures implemented in the Mantid (Arnold et al., 2014) software suite. The measured intensity was corrected for scattering contribution from the solvent and empty cells, azimuthally averaged to $I(q)$ *vs.* q and placed on an absolute scale.

2.10 Data fitting

SAXS and SANS data were simultaneously fitted using the Igor NIST analysis macro suite (Kline, 2006) and applying a two-level unified model. This model considers that, for each individual level, the scattering intensity is the sum of a Guinier term and a power-law function (Beaucage, 1995, 1996):

$$I(q) = \sum_{i=1}^{N} G_i \exp\left(-q^2 \cdot \frac{R_{g,i}^2}{3}\right) + \frac{B_i\left[\mathrm{erf}(qR_{g,i}/\sqrt{6})\right]^{3P_i}}{q^{P_i}} + bkg \qquad (3)$$

where $G_i = c_i V_i \Delta SLD_i{}^2$ is the exponential prefactor (where V_i is the volume of the particle and ΔSLD_i is the scattering length density (SLD) contrast existing between the i^{th} structural feature and the surrounding solvent), $R_{g,i}$ is the radius of gyration describing the average size of the i^{th} level structural feature, B_i is a q-independent prefactor specific to the type of power-law scattering with power-law exponent, P_i, and bkg is the background. In this

particular case, the largest structural level was modelled only by a power-law (R_{g1} was fixed at a value >> q_{min}^{-1} of 5000 Å). The radius of gyration for the second structural level (R_{g2}) was linked for all the SAXS and SANS data from the same sample and the background values were fixed for each sample.

3. Results and Discussion

3.1 Composition of the agar-based extracts

Different protocols, based on heat and combined heat-sonication treatments, with (samples coded as NaOH+HW and NaOH+HW-US) and without alkaline pre-treatment (samples coded as HW and HW-US), were applied to generate the agar-based extracts used in this work. As expected, large differences in the composition of the generated extracts existed (cf. Table 1). While the alkaline pre-treatment removed a significant fraction of the non-agar components present in the native seaweed and yielded extracts with higher carbohydrate contents, the extracts generated without applying the pre-treatment step presented a more heterogeneous composition, containing significant amounts of ash and proteins. Similar extracts from the same batch of *Gelidium* have been previously reported to contain minor amounts of polyphenols and lipids (Martínez-Sanz, Gómez-Mascaraque, et al., 2019). It is also interesting to note that, as previously reported (Martínez-Sanz, Gómez-Mascaraque, et al., 2019), the application of the combined heat-sonication treatment seemed to promote the extraction of other non-agar components (such as proteins), while it gave rise to lower carbohydrate contents in the extracts, most likely due to the reduced extraction time used. As expected, the results from the elemental analysis (see Table S1 from the Supplementary Material) showed that the agars produced with the alkali pre-treatment had the lowest sulphur content, comparable to a commercial agar produced from the same *Gelidium* source. It is reasonable to suggest that a major part of the sulphur in the non-alkali treated samples

was derived from alkali-labile sulphate; however, the high DS values estimated for these samples would suggest the presence of dominating $(L6S\text{-}G)_n$ structures, which are very unlikely to be found. Thus, the high sulphur content in the HW and HW-US extracts must also arise from the presence of other constituents such as co-isolated pigments and proteins. A greater content of sulphur/sulphate and charged polymers will further influence the level of minerals acting as counter ions of these constituents.

In line with previous works (Martínez-Sanz, Gómez-Mascaraque, et al., 2019; Murano et al., 1992), the alkali-treated samples presented lower weight average molecular weight (Mw) values than the non-purified extracts (cf. Table 1). This has been proposed to arise from the pre-treatment conditions being too harsh for the *Gelidium* seaweed, degrading part of the native agar (Martínez-Sanz, Gómez-Mascaraque, et al., 2019). On the other hand, the use of sonication also led to a decrease in the Mw of the extracts. This is not surprising, since both agar and carrageenan are prone to hydrolysis and depolymerisation at extended heating and energy input, especially due to the lability of 3,6-anhydro (LA or DA) residues (Sousa et al., 2012). However, it should be noted that the extracts produced in the present work had a higher molecular weight than the commercial agar used as a positive control or than values reported in the literature (Rochas & Lahaye, 1989), proving that the applied extraction procedures were not strongly degradative.

The constituent sugar analysis (cf. Table 2) revealed the common structural elements previously identified in agar from *Gelidium* seaweed, including O-methyl substitutions (Mouradi-Givernaud, A, Givernaud, Morvan, & Cosson, 1992). Alkali-labile precursor elements (L6S) were not positively identified as such, since they cannot be discriminated from 3-linked regular galactose (G-units) in the GC-based analysis. However, the high

sulphur content in the HW and HW-US extracts suggests the presence of such elements in these samples. As already anticipated, the agar content in the alkali-treated extracts was much higher than in their non-purified counterparts. The lower agar purity in the alkali-treated extracts, as compared to the commercial sample may be explained by the degradation of the agar during the alkali treatment and the co-extraction of some impurities which were not completely removed during the several washing steps of the extraction protocol. A striking result is the higher content of methylated sugars (LA2M and G6M) in the alkali-treated extracts, which suggests that agar fractions with such structural elements are more strongly embedded in the matrix and became more accessible after alkali treatment. All samples contained a small amount of glucose, which can be attributed to the presence of floridean starch, a storage polysaccharide which is commonly co-extracted with the agar (Carmona, Vergara, Lahaye, & Niell, 1998). Furthermore, as previously reported (Mouradi-Givernaud, Aziza, Hassani, Givernaud, Lemoine, & Benharbet, 1999), some xylose was detected in all samples; however, the same authors also detected the presence of rhamnose, of which we found no evidence in GC-MS analysis of alditol acetates. Compositional differences have been seen to have an impact on the functional properties of hydrogels and films produced from agar-based extracts (Martínez-Sanz, Gómez-Mascaraque, et al., 2019; Martínez-Sanz, Martínez-Abad, et al., 2019), which will ultimately determine the range of applications for which these materials may be suitable. To understand the structural implications, a complete rheological and nanostructural characterization of the agar-based hydrogels was carried out in this work.

Table 1. Basic composition and molecular weight data of the agar-based extracts.

	Carbohydrate (%) *	Protein (%)	Ash (%)	Sulphur (%)	DS (%)	Mw (kDa)	PI (Mw/Mn)

Commercial	83	1.49 ± 0.07[a]	4.3 ± 0.5[a]	0.70 ± 0.03[a]	0.070 ± 0.001 [a]	196	2.0
HW	42	10.55 ± 0.51[d]	34.7 ± 1.5[c]	2.22 ± 0.07[b]	0.32 ± 0.03[b]	840	1.7
HW-US	30	11.33 ± 0.42[d]	36.4 ± 0.9[c]	3.27 ± 0.08[c]	0.53 ± 0.01[c]	485	2.8
NaOH+HW	66	4.01 ± 0.08[b]	11.9 ± 2.1[ab]	0.63 ± 0.01[a]	0.08 ± 0.01 [a]	487	2.9
NaOH+HW-US	51	7.31 ± 0.07[c]	13.9 ± 3.9[b]	0.65 ± 0.02[a]	0.07 ± 0.02 [a]	265	1.7

Values with different letters are significantly different ($p \leq 0.05$). Data were analyzed by ANOVA followed by a Tukey-test.

DS: degree of sulphate substitution; Mw: weight-average molecular weight; PI: polydispersity index.

*The total gross carbohydrates were estimated as the sum of the agar, glucose and xylose contents (cf. Table 2).

Table 2. Carbohydrate composition of the agar-based extracts. The results are expressed as g polysaccharide per 100 g dry weight sample.

	LA	G	LA2M	G6M	Agar	Glc	Xyl
Commercial	34.0 ± 0.1[d]	42.9 ± 0.01[d]	2.8 ± 0.1[c]	0.4 ± 0.1[a]	80	1.5 ± 0.1[a]	0.9 ± 0.1[ab]
HW	15.6 ± 0.5[b]	23.3 ± 0.3[ab]	1.0 ± 0.2[a]	0.8 ± 0.03[b]	40	2.0 ± 0.3[a]	0.8 ± 0.01[a]
HW-US	8.5 ± 0.8[a]	19.1 ± 0.8[a]	0.5 ± 0.03[a]	0.1 ± 0.02[a]	28	1.8 ± 0.2[a]	0.7 ± 0.03[a]
NaOH+HW	23.8 ± 1.1[c]	32.4 ± 1.1[c]	6.4 ± 0.6 [b]	1.8 ± 0.1[c]	63	2.2 ± 0.1[a]	0.9 ± 0.02[ab]
NaOH+HW-US	15.9 ± 1.4[b]	25.5 ± 2.1[b]	6.2 ± 0.6 [b]	0.4 ± 0.1[a]	48	2.1 ± 0.2[a]	1.1 ± 0.1[b]

Values with different letters are significantly different ($p \leq 0.05$). Data were analyzed by ANOVA followed by a Tukey-test.

LA=3,6-anhydro-L-galactose; G=D-galactose; LA2M=2-O-methyl-3,6-anhydro-L-galactose; G6M=6-O-methyl-D-galactose; Glc=D-glucose; Xyl=xylose. Nomenclature is according to (Knutsen et al., 1994).

3.2 Rheological characterization of the agar-based extracts

To investigate the effect of the distinct composition on the gelation mechanism of the agar-based extracts, rheological experiments were carried out and representative results are presented in Figure 1. As observed, all the samples showed similar behaviour as a function of cooling. During cooling, an initial stage at which G' and G" remained almost constant was observed, followed by a sharp increase in both moduli when lowering the temperature below a certain value. The gelling and melting temperatures of agars are often estimated from the crossover point of G' and G" in cooling and heating ramps (Sousa et al., 2013). However, none of the agar-based samples, except for the commercial sample (for which the crossover point was detected at 45 ºC), presented a true solution behaviour (G">G'); instead they displayed behaviour typical of entangled networks at the initial temperature of 75 ºC, especially the purified alkali-treated samples. This behaviour has been previously observed for agarose (Mohammed, Hember, Richardson, & Morris, 1998) and agar (Alehosseini et al., 2018). Although agarose chains are known to associate by forming ordered helical structures, this observation does not necessarily mean that these helices were already formed at 75 ºC, but it implies the existence of some kind of molecular association. The greater molecular weights of all the agar-based extracts, as compared to the commercial agar, may explain the occurrence of more extensive molecular interactions in the former. As we did not observe a true cross-over between G">G', we defined the apparent gelling temperature by determining the point at which an abrupt rise in G' and G" took place, in line with other studies (Alehosseini et al., 2018; Russ, Zielbauer, Koynov, & Vilgis, 2013). This transition corresponds to the formation of a well-developed network by aggregation of the agarose helices into larger bundles, which have been previously related to the existence of strong gels (Indovina et al., 1979; Mohammed et al., 1998). As deduced from the values listed in Table 3, this transition took place within the range of 37-42 ºC for all the agar-based extracts. This is in agreement with the range of gelling temperatures typically reported in the literature

for agar and agarose samples (40-10 ºC), depending on the thermal history and cooling conditions (Aymard et al., 2001). Despite the lower agar contents in the HW and HW-US extracts, the temperatures at which gelation occured were only slightly decreased with respect to the commercial agar and alkali-treated samples. In fact, previous studies showed very little effect of the agarose concentration on the temperature at which aggregation of the double helices took place (Fernández et al., 2008; Millán, Moreno, & Nieto, 2002; Nordqvist & Vilgis, 2011). Moreover, this indicates that the presence of other components such as proteins in the non-purified extracts did not have a strong impact on the temperature at which the agarose helices aggregated to form hydrogels. After equilibration at 20 ºC, the samples were heated to 75 ºC. Raising the temperature led to a decrease in absolute value of G' and G". However, no real melting transition was observed for any of the samples (G">G'), indicating that the entanglements between the agar molecular chains were not completely disrupted during the heating run. It should be mentioned here that trials were made heating the samples up to 95°C without observing any melting transition; only a reduction in absolute values of moduli (results not shown) were found. A characteristic feature of all the agar-based hydrogels studied here is that they presented large thermal hysteresis (i.e. they showed large differences in their behaviour upon cooling and heating). This hysteresis is typical of agarose hydrogels and has been attributed to the formation of large aggregates of double helices, which remain stable at temperatures much higher than those at which they start associating on cooling (Indovina et al., 1979; Mohammed et al., 1998; Trefna & Ström, 2019). The difference between the cooling and heating curves seemed to be greater for the commercial agar and the NaOH+HW agar-based extract compared to the other samples. For instance, a significant difference was observed for these samples between the G' value of the freshly prepared solutions at 75 ºC at the beginning of the cooling ramp and G' at 75 ºC after gelation and subsequent heating ramp. A plausible explanation for this is that, due to the

greater agar content in these extracts (cf. Table 2), more stable aggregates of double helices were formed.

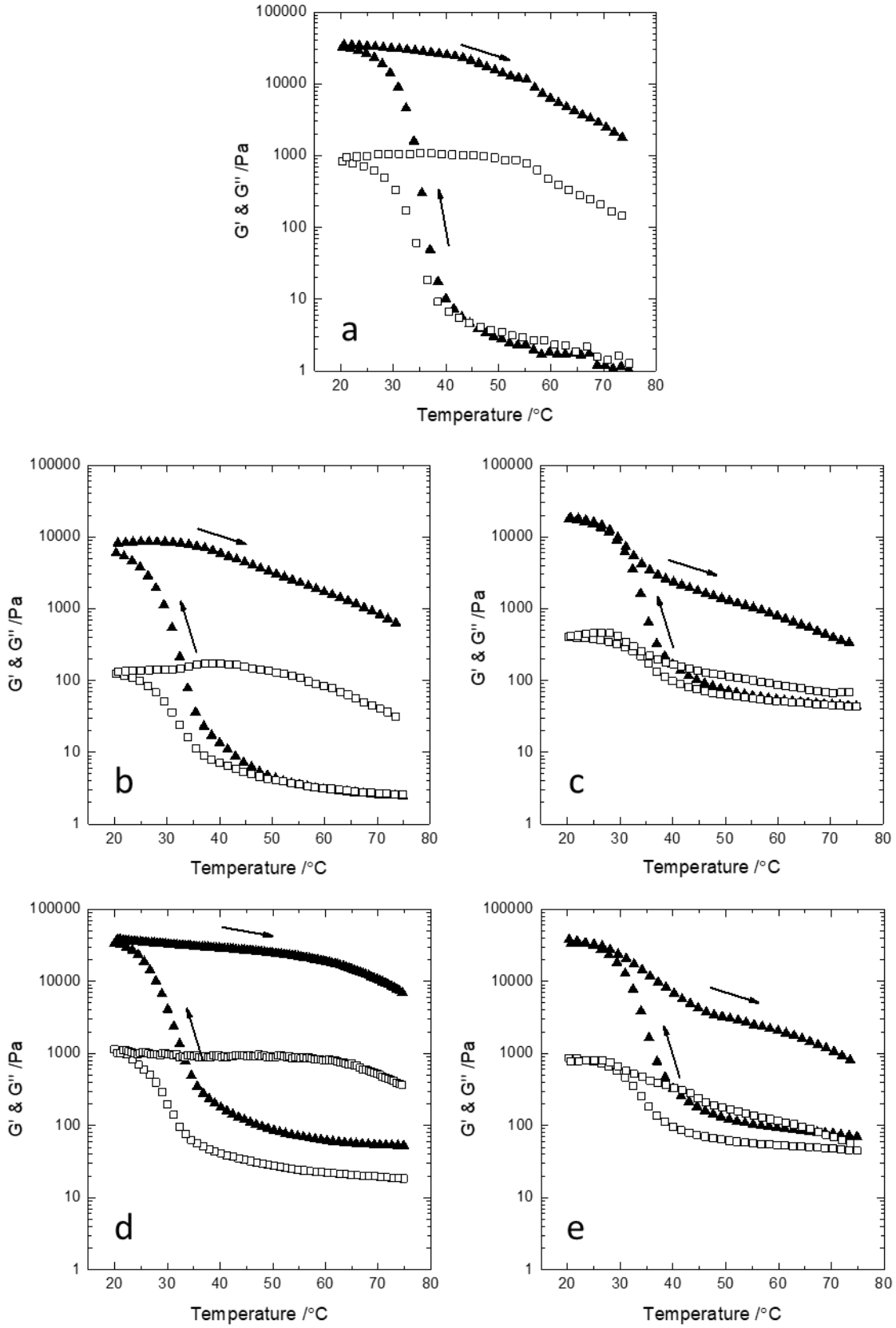
a
b
c
d
e
G' & G'' /Pa
Temperature /°C
100000
10000
1000
100
10
1
20
30
40
50
60
70
80

476

Figure 1. Temperature dependence of G' (filled triangles) and G" (open squares) moduli of agar-based extracts during cooling and heating ramps (arrows indicate the direction of the temperature ramps). (a) Commercial; (b) HW; (c) HW-US; (d) NaOH+HW and (e) NaOH+HW-US.

Table 3. Rheological and mechanical properties of the different agar-based extracts: Apparent gelation temperature ($T_{g'}$), elastic modulus ($G'_{20ºC}$), viscous modulus ($G''_{20ºC}$) and tan δ measured at 20ºC, maximum true stress (σ_{max}) and Young's modulus (E).

	$T_{g'}$ (ºC)	$G'_{20ºC}$ (kPa)	$G''_{20ºC}$ (kPa)	tan δ	σ_{max} (kPa)	E (kPa)
Commercial	40	25 ± 1^{c}	0.6 ± 0.1^{bc}	0.025 ± 0.005^{a}	29 ± 12^{ab}	21 ± 2^{a}
HW	39	18.7 ± 0.4^{b}	0.5 ± 0.1^{ab}	0.028 ± 0.006^{a}	10 ± 1^{a}	26 ± 5^{a}
HW-US	37	7.8 ± 0.4^{a}	0.20 ± 0.03^{a}	0.021 ± 0.006^{a}	5.6 ± 0.5^{a}	22 ± 4^{a}
NaOH+HW	42	39 ± 1^{d}	1.1 ± 0.1^{d}	0.028 ± 0.003^{a}	49 ± 6^{b}	28 ± 1^{a}
NaOH+HW-US	40	36 ± 2^{d}	1.01 ± 0.01^{d}	0.029 ± 0.007^{a}	39 ± 8^{b}	33 ± 3^{a}

Values with different letters are significantly different ($p \leq 0.05$). Data were analyzed by ANOVA followed by a Tukey-test.

To gain further insights on the rheological behaviour of the samples, frequency sweeps were recorded at a higher temperature (80 ºC) and at a lower temperature at which all the samples had undergone the transition to strong hydrogels (20 ºC). Representative plots, shown in Figure 2, demonstrate distinct behaviour of the samples at the two chosen temperatures. At 80 ºC, G' and G" were similar and increased with frequency, which is a behaviour typical of an entangled or weak gel-like network. In particular, no cross-over point (G"=G') was detected for the NaOH+HW agar-based extract, which presented a structure characteristic of an entangled network within the whole frequency range. At 20 ºC, all the samples showed

behaviour typical of strong hydrogels, where G' was at least one order of magnitude higher than G" and both moduli were independent of the frequency within the studied range (0.1–100 rad/s). The average values for G' and G" at 20 ºC, listed in Table 3, indicate that the HW and HW-US extracts, as expected given the presence of other non-agar components, produced hydrogels with lower absolute values for G' and G". On the other hand, the tan δ (tan δ=G"/G') values were similar for all samples (ca. 0.02-0.03), showing comparable amount of elastic response. The most likely explanation is that the presence of other components in the HW and HW-US extracts did not have a dramatic impact on the nature of the interactions established between the agarose chains (i.e. the gelling fraction of the material); however, they did lead to the formation of softer hydrogels mainly due to the lower agar (and agarose) content (i.e. fewer or smaller agarose aggregates, responsible for holding the hydrogel network structure, were formed).

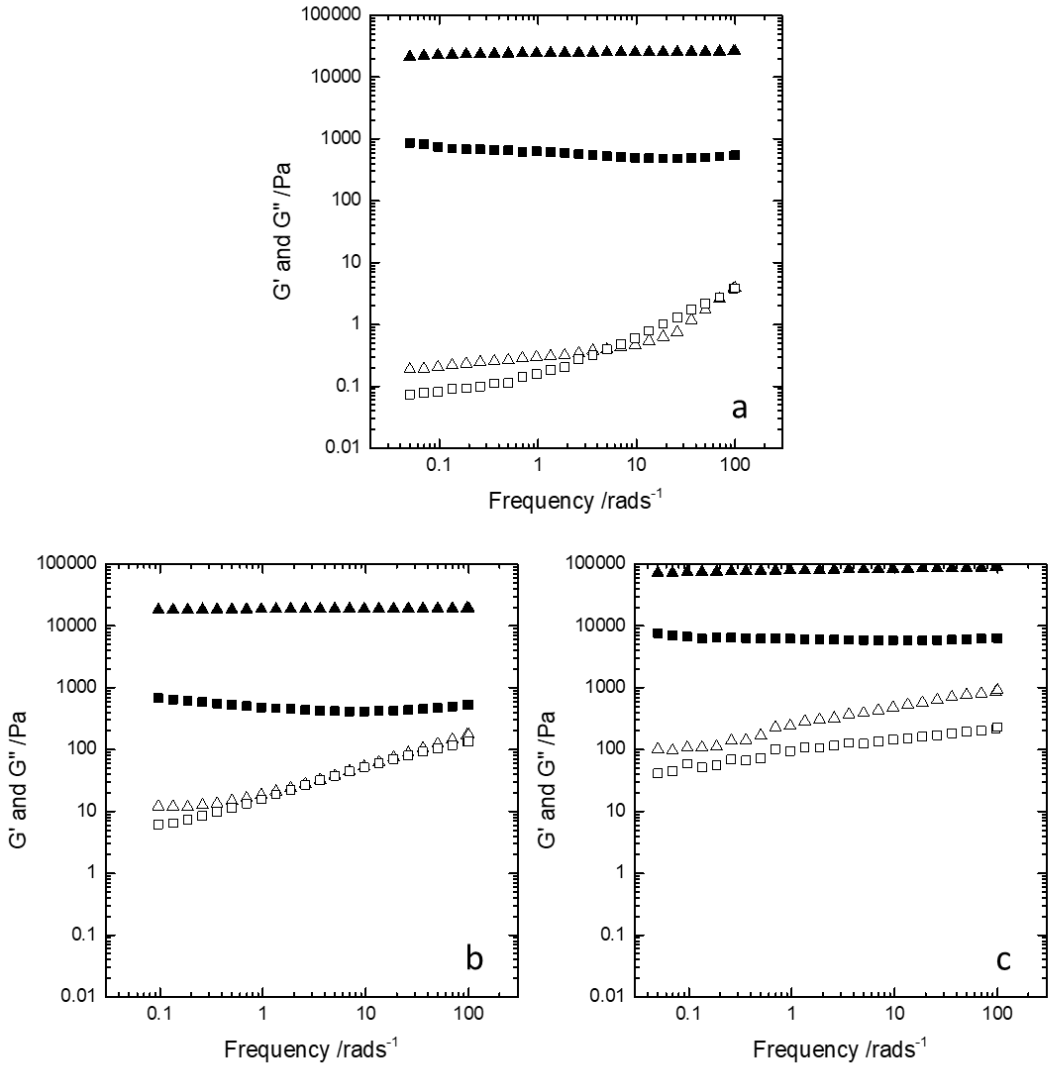

509

510 **Figure 2.** G' (triangles) and G" (squares) as a function of frequency for the agar-based
511 extracts, measured at temperatures of 80 ºC (open symbols) and 20 ºC (filled symbols). (a)
512 Commercial; (b) HW and (c) NaOH+HW.

513

514 In the compression tests (cf. Figure S1) two regions were observed in the plots of all the
515 hydrogels: (i) a short linear stress-strain region and (ii) a region were stress increased more
516 markedly until the gel fractured, represented by a peak in the curve. The first linear region
517 extended up to strains of ca. 30 % for the commercial agar and the NaOH+HW and
518 NaOH+HW-US extracts, whilst this region was shorter (up to ca. 20 %) for the HW and

519 HW-US extracts. Linearity from strains of 15 % up to the fracture point has been previously
520 reported for agar gels (Nakauma, Ishihara, Funami, Yamamoto, & Higashimori, 2014). As
521 deduced from the parameters listed in Table 3, the hydrogels from the alkali pre-treated
522 extracts were the hardest ones, since they presented the greatest maximum true stress values.
523 On the contrary, and in agreement with the rheological characterization, the presence of other
524 components such as proteins in the less purified extracts gave rise to the formation of softer
525 hydrogels. The highest true stress values for the hydrogels from the alkali pre-treated extracts
526 could be related to (i) the inherent higher agar (and agarose) fraction, (ii) the greater
527 molecular weight of the agar (compared with the commercial grade) and (iii) the lower
528 sulphate content in these extracts. The negative impact of higher sulphate contents in the
529 strength of agar hydrogels (Kumar & Fotedar, 2009; Yousefi, Islami, & Filizadeh, 2013), as
530 well as the ability of alkali pre-treatments to remove sulphate groups from the galactose units
531 (Matsuhiro & Urzúa, 1990) have been widely described in the literature. However, our
532 results demonstrate that the purity and molecular weight of the agar are also critical factors
533 affecting the mechanical performance of agar-based hydrogels. The Young's modulus was
534 estimated from the linear slope of the true stress-strain curves. The modulus of the
535 commercial agar (ca. 21 kPa) was within the range of values previously reported (Ross,
536 Pyrak-Nolte, & Campanella, 2006; Sharma & Bhattacharya, 2014). On the other hand,
537 although minor differences were detected between all the agar-based extracts, the alkali-
538 treated agars seemed to produce the stiffest hydrogels. This might be related to the formation
539 of thicker junction zones in the case of these samples, as later confirmed by the scattering
540 results, particularly in the NaOH+HW hydrogel.
541

3.2 Nano- and micro-structure of agar gels: Small angle X-ray scattering characterisation

The different rheological and mechanical behaviour of the agar-based hydrogels were expected to arise from structural differences in the nano- and micrometre scale. Thus, to characterize the native structure of the agar-based hydrogels, SAXS and SANS experiments were carried out. Figure 3A-E shows the experimental data from the SAXS and SANS contrast variation experiments. In general, the shape of the scattering curves was similar to that previously observed for 1-5% w/v agarose hydrogels (Fatin-Rouge, Wilkinson, & Buffle, 2006; Krueger et al., 1994), where three different regions were distinguished: (i) domain I ($q = 0.0023-0.015$ Å^{-1}) where the scattering intensity for most of the samples showed a power-law behaviour, (ii) domain II ($q = 0.015-0.1$ Å^{-1}) where the curves showed a shoulder-like feature, and (iii) domain III ($q = 0.1-0.9$ Å^{-1}) where the SANS curves were mostly dominated by the incoherent scattering arising from the presence of hydrogen atoms in the agar gel structure. The SAXS and SANS scattering curves from the H_2O-soaked gels were not analogous, showing a marked difference within the region $q < 0.005$ Å^{-1}, where the SAXS curves presented a much more marked increase in the scattering intensity. This may be a consequence of the increased interfacial surface scattering existing between the agarose component in the hydrogels and water when using X-rays ($\Delta SLD_{SAXS} = 5.85$ cm^{-2}) compared to the case for neutrons ($\Delta SLD_{SANS} = 2.72$ cm^{-2}) as the source of radiation (cf. Table S2 from the Supplementary Material for reference values of the scattering length densities from agarose and water), and noting that the intensity is proportional to the square of the contrast i.e. 4.6 times greater for SAXS.

No specific fitting models have been applied to small angle scattering data from agar and agarose hydrogels in the existing literature and data analysis has been mostly limited to the

567 determination of power-law exponents and cross-sectional radii (Djabourov et al., 1989;
568 Krueger et al., 1994; Rochas et al., 1999; Singh, Aswal, & Bohidar, 2007, 2009).
569 Alternatively, a model based on the combination of two populations of rod-like particles
570 with different diameters was applied to the SAXS data from agarose gels, although the fits
571 were not completely satisfactory (Djabourov et al., 1989). More recently, a correlation length
572 model was successfully applied to describe the SANS data from agarose hydrogels cross-
573 linked with Ca^{2+} (Fatin-Rouge et al., 2006). The correlation length model was also applied
574 to fit the data presented in this work; however, such model was not successful to
575 simultaneously fit the SAXS and SANS contrast variation data from the different agar-based
576 hydrogels. Alternatively, an empirical unified model was used. This model provided
577 satisfactory fits (cf. Figures 3A-E), except for the low q region ($q < 0.005$ Å^{-1}) in the SAXS
578 patterns where the fitting curves deviated from the experimental data (results not shown).
579 The power-law exponents from the domain I (P_1) and the radii of gyration (R_{g2}), estimated
580 from the scattering intensity within the domain II, are summarized in Table 4 (the complete
581 compilation of all the fitting parameters for each sample can be found in Tables S3-S7 of the
582 Supplementary Material). As observed, the power-law exponents for the SAXS patterns
583 were significantly greater than those from the SANS data. This is most likely due to the
584 distinct SLD contrast generated by X-rays and neutrons and to the fact that the low q region
585 in the SAXS data was affected by the presence of large-scale scattering features. Even with
586 this straightforward empirical model, the experimental SAXS data were not well described
587 within the lowest q region. According to the size range corresponding to this low q region
588 (>130 nm), the occurrence of these scattering features may be associated with the hydrogel
589 network structure in the agar samples. A plausible hypothesis would be the existence of a
590 porous structure with core-shell regions, which would provide different slopes for SAXS
591 and SANS. Such core-shell regions, leading to a reduced slope in the low q region, could

arise as a consequence of differences in solvent accessibility between different regions within the sample during solvent exchange treatment when the samples are soaked in D_2O/H_2O, resulting a consequent variations in OH/OD exchange; this is similar to what has been reported previously for cellulose hydrogels (Lopez-Sanchez et al., 2017; Martínez-Sanz, Gidley, & Gilbert, 2016; Martínez-Sanz, Mikkelsen, et al., 2016). Irrespective of its origin, extending the lower q region, i.e. with USAXS/USANS, would be desirable to analyse the data within this region and extract reliable structural information. Supporting the above, the power-law exponents from the SANS patterns varied depending on the sample and on the SLD contrast generated by the different D_2O/H_2O mixtures used. The commercial agar presented exponents of 1.8-1.9 which are similar to the value of 1.7 previously reported for agarose hydrogels (Fatin-Rouge et al., 2006) and consistent with the existence of structures analogous to swollen linear chains in a solvent that is intermediate between a good and theta solvent (Yang et al., 2016). The scattering profile of SANS data for hybrid agar-gelatin hydrogels in the q range of 0.007-0.02$Å^{-1}$ also showed a power-law behaviour with an exponent of 1.6 for the highest agar ratio (Santinath Singh, Aswal, & Bohidar, 2011). This was attributed to the existence of rod-like structures consisting of agarose double-helix aggregates. The associated radius of gyration was 5.6 nm for the commercial agar (very similar to the correlation length of 5.9 nm previously reported for agarose gels) and was attributed to the thickness of the bundles of agarose double helices (Fatin-Rouge et al., 2006). Interestingly, the power-law exponents for all the agar-based hydrogels were higher than for the commercial agar, with values between ca. 1.9 and 2.9. This is indicative of more branched structures (which is most likely due to a greater degree of chain association or cross-linking) in the case of the produced agar-based hydrogels, which can be correlated with their greater molecular weights. A similar increase in the power-law exponents of agarose hydrogels was observed when increasing the agarose concentration; this was

hypothesised to arise from either lower swelling of the junction zones (i.e. agarose bundles) at greater agarose concentrations or from changes in the large-scale structure of the agarose hydrogel network (an decrease in the pore size at higher agarose concentrations) (Krueger et al., 1994). While the radius of gyration slightly decreased for the non-purified agar-based hydrogels (5.0 nm for HW and 4.6 nm for HW-US), larger values were obtained for the purified hydrogels (9.6 nm for NaOH+HW and 6.7 nm for NaOH+HW-US). These results would suggest a greater extent of chain association in the alkali-treated agar-based hydrogels, which may be directly linked to their greater agar content and lower sulphate content. On the contrary, the lower agar content in the HW and HW-US hydrogels led to the formation of smaller aggregates, although the presence of other components did not seem to impair the interconnectivity in the hydrogel network, as suggested by the corresponding power-law exponents. The existence of thicker agarose bundles or aggregates in the alkali-treated agar hydrogels is in agreement with the compression experiments, which showed a stiffer behaviour for these samples as compared to the commercial agar and the HW and HW-US hydrogels.

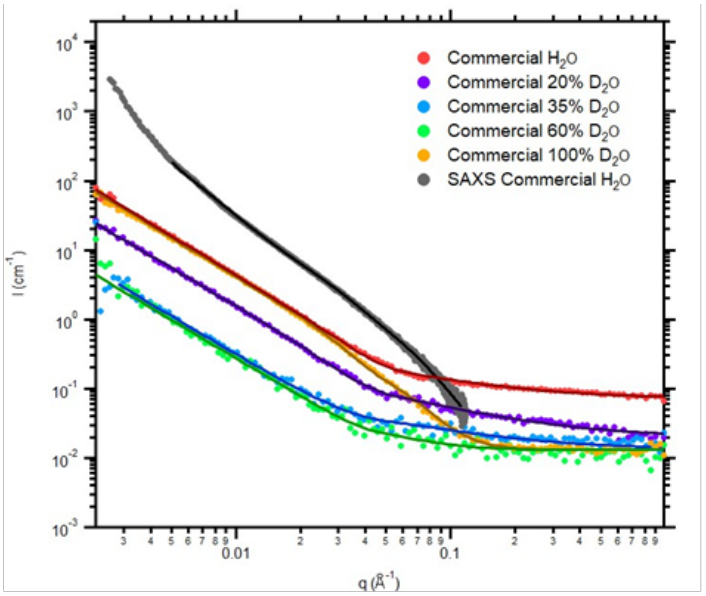
Commercial H_2O
Commercial 20% D_2O
Commercial 35% D_2O
Commercial 60% D_2O
Commercial 100% D_2O
SAXS Commercial H_2O
I (cm^{-1})
q (Å^{-1})

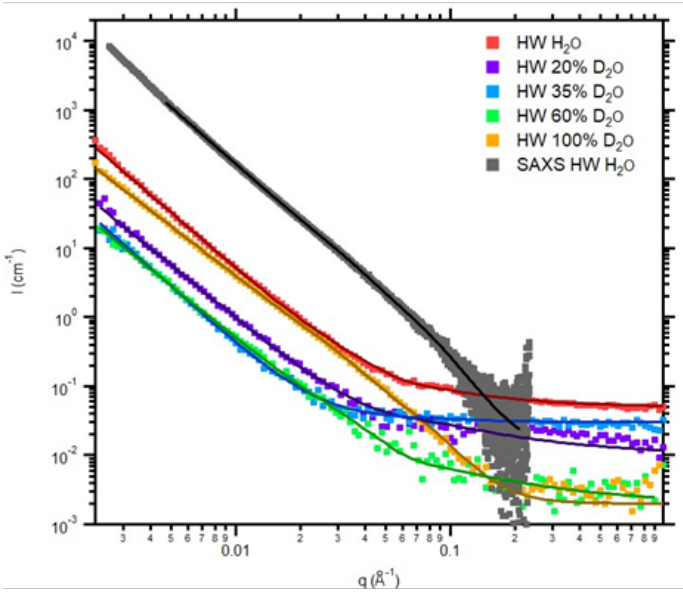
HW H_2O
HW 20% D_2O
HW 35% D_2O
HW 60% D_2O
HW 100% D_2O
SAXS HW H_2O
I (cm^{-1})
q (Å^{-1})

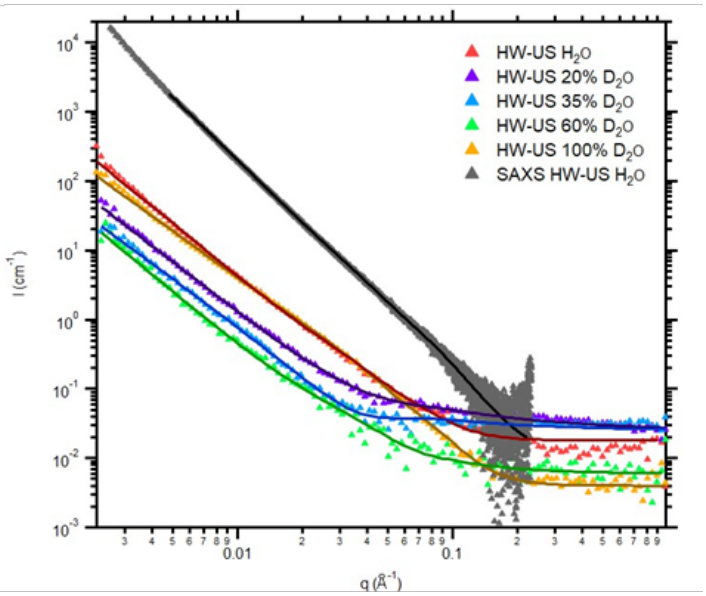
HW-US H_2O
HW-US 20% D_2O
HW-US 35% D_2O
HW-US 60% D_2O
HW-US 100% D_2O
SAXS HW-US H_2O
I (cm^{-1})
q (Å^{-1})

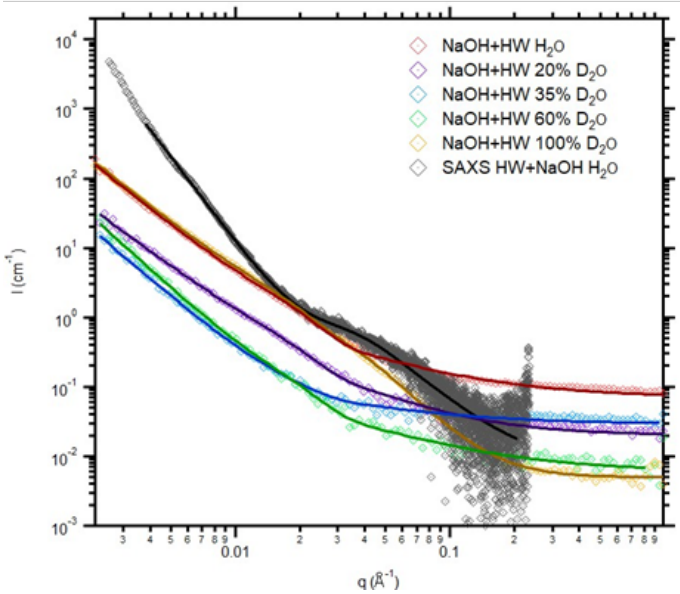
NaOH+HW H_2O
NaOH+HW 20% D_2O
NaOH+HW 35% D_2O
NaOH+HW 60% D_2O
NaOH+HW 100% D_2O
SAXS HW+NaOH H_2O
I (cm^{-1})
q (Å^{-1})

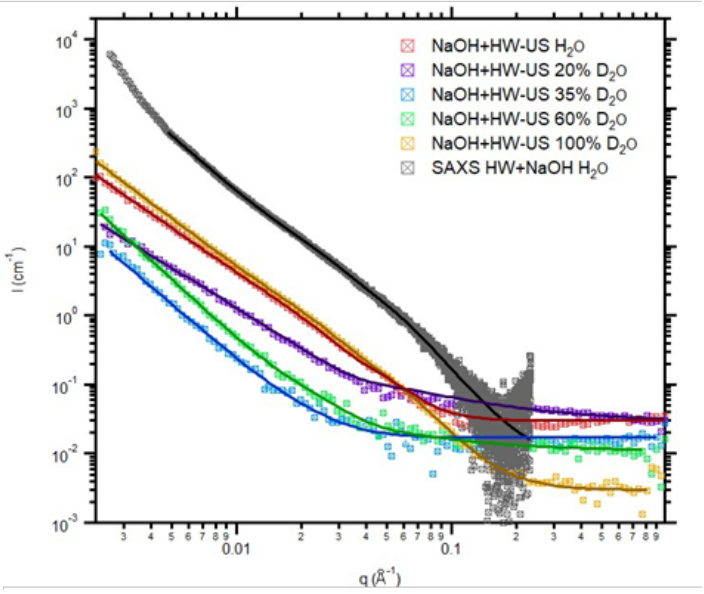
NaOH+HW-US H_2O
NaOH+HW-US 20% D_2O
NaOH+HW-US 35% D_2O
NaOH+HW-US 60% D_2O
NaOH+HW-US 100% D_2O
SAXS HW+NaOH H_2O
I (cm^{-1})
q (Å^{-1})

633

Figure 3. SAXS and SANS contrast variation data for the agar-based hydrogels. Dots represent the experimental data and solid lines show the fits obtained by applying the two-level unified model and simultaneously fitting the six data sets.

Table 4. Fit parameters and contrast values for the SAXS and SANS data from the agar-based hydrogels. Parameters obtained from the fits of the unified model are power-law exponents (P_1) and radii of gyration (Rg_2); contrast match point and scattering length density (SLD) values have been estimated from the SANS contrast variation experiments.

	Commercial	HW	HW-US	NaOH+HW	NaOH+HW-US
P_1 (SAXS)	2.6	2.7	3.0	3.9	2.7
P_1 (SANS)	1.8-1.9	2.4-2.7	2.3-2.6	2.3-2.8	1.9-2.9
R_{g2} (nm)	5.6	5.0	4.6	9.6	6.7
Contrast match (% D_2O)	52 ± 1	54.4 ± 0.8	53.0 ± 0.4	48.0 ± 0.2	44 ± 2
SLD (10^{10} cm^{-2})	3.01 ± 0.08	3.19 ± 0.05	3.09 ± 0.02	2.75 ± 0.01	2.5 ± 0.1

The SLD of the agar-based hydrogels could be estimated, in principle, from the SANS contrast variation experiments by determining the contrast match point. The scattering intensity at several points within the q range of 0.0025-0.0055$Å^{-1}$ was determined for each of the five different D_2O/H_2O mixtures used in the experiments and the values were plotted against the D_2O content. If no deviations from the theoretical behaviour occur (i.e. the samples are pure and there is no H/D exchange taking place), the so-obtained values should be properly described by a parabolic function and the intensity should reach a minimum of zero at the contrast match point for a single phase system. As observed in Figure 4A, for most of the samples the experimental data deviated from the theoretical parabolic function, with this effect being more evident in the case of the HW and HW-US hydrogels. Such a

deviation from the theoretical behaviour is not surprising, since the agar-based hydrogels are highly hydrated systems (up to 98% water) in which H/D exchange may have occurred when the samples were soaked in D_2O/H_2O. In fact, similar behaviour has been reported for highly hydrated polysaccharide gels such as cellulose-based hydrogels (Martínez-Sanz, Gidley, et al., 2016; Martínez-Sanz, Mikkelsen, et al., 2016). The contrast match point value for each agar-based hydrogel, listed in Table 4, was calculated from the minimum of the intensity in the fitted parabolic functions. Considering that at the contrast match point the solvent SLD equals that of the sample, the neutron SLD of the agar-based hydrogels could be estimated by applying the following equation:

$$SLD_{Agar} = SLD_{solvent} = (x_{D2O} \cdot 6.38 \cdot 10^{10}) + \left((1 - x_{D2O}) \cdot (-0.56 \cdot 10^{10})\right) \quad (4)$$

On the other hand, the theoretical SLD value for pure agarose (considering a molecular formula of $C_6H_{10}O_5$ (Ramzi, Rochas, & Guenet, 2000)) can be estimated using the following expression:

$$SLD_{Agarose} = N_A \cdot \rho_{Agarose} \cdot \frac{12b_C + 9b_O + 18b_H}{12M_C + 9M_O + 18M_H} = 2.16 \cdot 10^{10} \text{ cm}^{-2} \quad (5)$$

where b_i and M_i are the neutron scattering length and mass of the atoms, respectively and $\rho_{Agarose}$, is the physical density of agarose (1.7 g/cm^3 (Rochas et al., 1999)).

Considering that (i) the structure of agar differs from the idealized agarose structure and it contains substituents along the molecular chains (giving rise to more defective regions, with lower physical density) and (ii) the hydrogels contain a high amount of water, it would be expected that the agar-based hydrogels should present lower SLD values than that of pure agarose. Surprisingly, as deduced from Table 4, the SLD from all the samples was greater than that of pure agarose. This was more evident in the case of the HW and HW-US hydrogels, which could be originated from the deviation of the contrast variation curves from

the theoretical behaviour, induced by a greater H/D exchange taking place in these samples, as latter commented in the text. In the case of the more purified agars, the NaOH+HW-US and NaOH+HW extracts presented SLD values closer to that of agarose, as compared to the commercial agar. This might indicate that the increase in the calculated SLD values arise from the deviation of the contrast variation curves from their theoretical behaviour due to H/D exchange. Such an exchange process would be more limited in the alkali-treated extracts due to their greater molecular weight and crystallinity (Martínez-Sanz, Gómez-Mascaraque, et al., 2019), hence affecting to a lesser extent the shape of their contrast variation curves.

To estimate the degree of H/D exchange taking place in the agar-based hydrogels, the theoretical contrast variation curves for pure agarose at different degrees of exchange were calculated and compared to the experimental data from the pure agar hydrogels. When an agarose hydrogel is soaked in D_2O, a maximum of four hydrogen atoms, corresponding to the labile hydroxyl groups, can be exchanged; thus the molecular formula of fully exchanged agarose would be $C_{12}H_{14}D_4O_9$. Accordingly, for certain intermediate degree of H/D exchange ($exc_{H/D}$) the SLD can be estimated as follows:

$$SLD_{Agarose\ fully\ exc} = N_A \cdot \rho_{Agarose} \cdot \frac{12b_C+9b_O+(18-(4\cdot exc_{H/D}))b_H+(4\cdot exc_{H/D})b_D}{12M_C+9M_O+\left(18-\left(4\cdot exc_{H/D}\right)\right)M_H+(4\cdot exc_{H/D})M_D} \quad (6)$$

Equally so, for a D_2O volume fraction, x_{D_2O}, of 0.5, complete exchange would result in two labile H atoms being replaced by D. Hence, combining equations (5) and (6), the resultant theoretical SLD of agarose in each D_2O/H_2O mixture may be calculated by applying the following equation:

$$SLD_{Agarose\ exc} = x_{D_2O} \cdot SLD_{Agarose\ fully\ exc} + (1 - x_{D_2O}) \cdot SLD_{Agarose} \quad (7)$$

for degrees of H/D exchange with the solvent varying between 0 and 1.

Figure 4B shows the theoretical curves for the term $\left(SLD_{Agarose} - SLD_{solvent}\right)^2$ plotted against the D_2O volume fraction, considering different degrees of H/D exchange, as well as the experimental data points for the pure agar hydrogels. The first clear observation is that, as already anticipated, the contrast match point is shifted towards greater D_2O volume fractions with greater H/D exchange ratios. This would explain the fact that the shape of the contrast variation curves for the agar hydrogels deviated from the 0% H/D exchange curve, especially for greater D_2O volume fractions, becoming closer to the 100% H/D exchange curve. Moreover, it can be observed how the behaviour of the more crystalline samples (NaOH+HW-US and NaOH+HW) deviate to a lesser extent from the 0% H/D exchange curve; in this case, and as suggested by the rheological characterization, thicker and more stable agarose bundles were formed, consistent with reduced levels of H/D exchange.

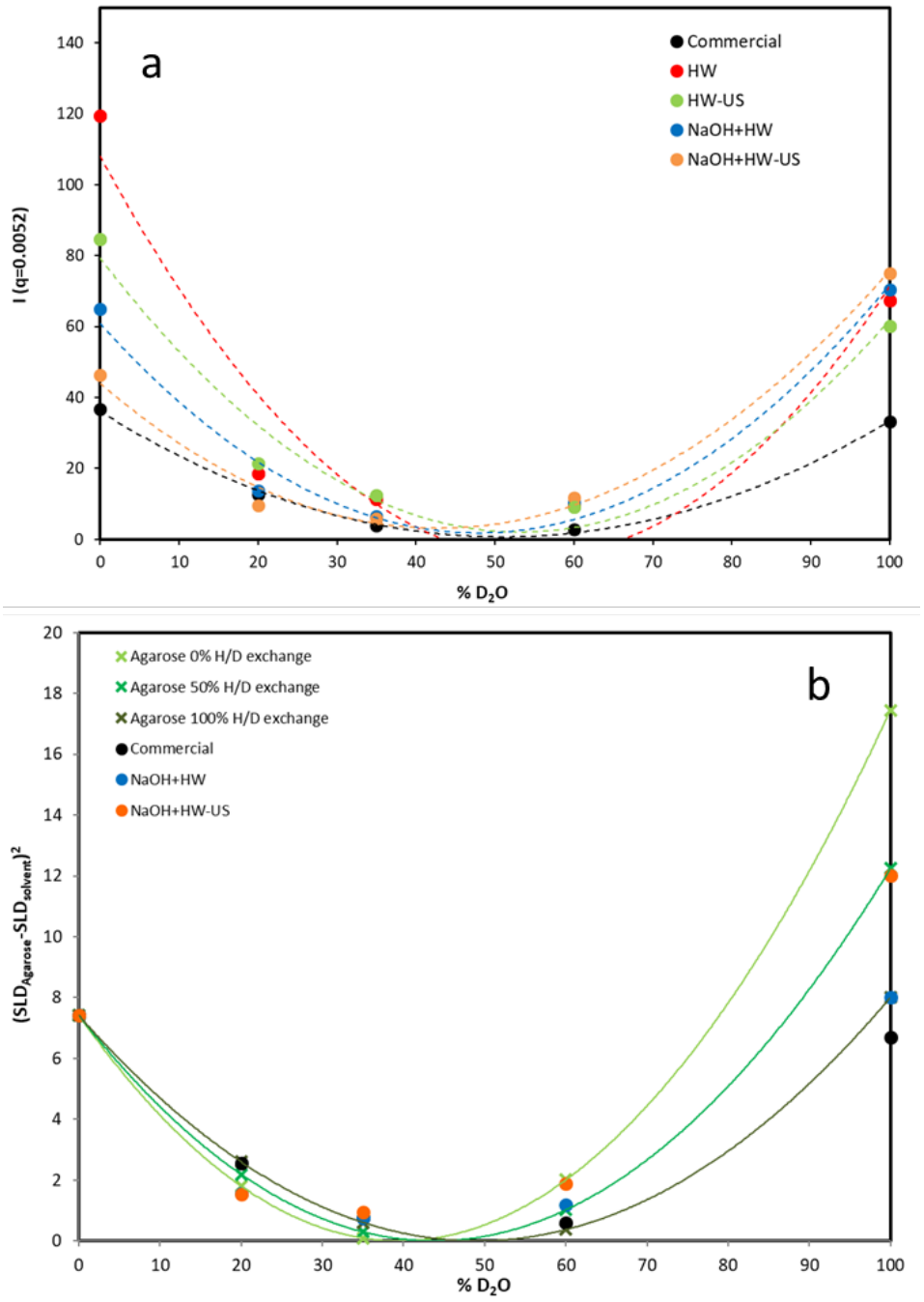

714

715 **Figure 4.** (a) Contrast variation curves for the agar-based extracts, obtained from the SANS
716 experiments. Solid markers represent the experimental values ($q=0.0052Å^{-1}$) and dotted
717 lines correspond to the fitted parabolic functions. (b) Representation of the scattering length
718 density contrast term $(SLD_{Agarose}-SLD_{solvent})^2$ as a function of the D_2O content of the
719 different solvent mixtures used for the contrast variation experiments. Dots represent the
720 experimental values for the agar gels and crosses represent the theoretical values calculated

721 by assuming different degrees of H/D exchange; solid lines correspond to the fitted
722 parabolic functions.
723
724 To further investigate the structural changes undergone by the agar-based extracts during the
725 gelation and melting processes, temperature-resolved SAXS experiments were also carried
726 out. The complete set of curves for the heating and cooling ramps can be found in the
727 Supplementary Material section (Figures S2 and S3, respectively). For clarity, only selected
728 curves (those corresponding to the 25 ºC and 95 ºC curves obtained during the heating and
729 cooling ramps) were used to generate the Kratky plots shown in Figure 5. As observed, the
730 Kratky plots highlighted the appearance of small humps located at ca. 0.006 $Å^{-1}$ in the SAXS
731 curves from most of the samples. The position and intensity of these features were unaffected
732 by the temperature treatments, although they were less evident in the HW and HW-US
733 samples. The appearance of such features has not been reported before and it is unclear as to
734 whether they are characteristic of form or structure factor effects. A possible origin may be
735 a form factor effect associated with the length of the agarose double helices, whose
736 concentration was greater in the more purified samples and whose structure was not altered
737 during the heating/cooling steps. Again, extending the q range would be desirable to discard
738 any other possible sources such as a structure factor effect derived from the interaction
739 between the agarose bundles or a structure factor effect related to the larger scale porous
740 structure. In general, the scattering intensity is seen to decrease when raising the temperature
741 above a certain point during the heating runs. This may have arisen from a drop in the SLD
742 contrast between the hydrogels and the surrounding solvent due to a decrease in the cross-
743 linking degree of the hydrogels (i.e. disassociation of agarose bundles). This temperature
744 corresponded to ca. 55 ºC for the commercial agar, 65 ºC for NaOH+HW-US and 85 ºC for
745 HW, HW-US and NaOH+HW. The reduction in the scattering intensity was more obvious

746 in the case of the commercial agar; in contrast, the intensity of the NaOH+HW agar-based
747 hydrogel remained almost unaffected. This again could be related to the formation of thicker
748 and more stable aggregates in the latter. Moreover, the shoulder-like feature associated with
749 the presence of agarose double-helix aggregates (located within the range of q = 0.015−0.1
750 $Å^{-1}$) was absent in the scattering patterns from the samples at 95 ºC, except for the
751 NaOH+HW agar-based hydrogel. Since no true melting behaviour was observed in the
752 rheological experiments (cf. Figure 1), the results from the SAXS heating ramps suggest that
753 although the molecular associations between agarose chains (i.e. agarose double-helix
754 structures) were not destroyed upon heating, the double-helix aggregates, responsible for the
755 formation of strong hydrogel networks, were disrupted in most of the samples. In the
756 particular case of the NaOH+HW agar-based hydrogel, it seems that very strong interactions
757 must have been formed between the agarose double helices, leading to the formation of more
758 stable agarose bundles which remained intact even at 95 ºC. This is in agreement with the
759 rheological characterization where, after heating to 70 ºC, the G' and G'' moduli still
760 produced much higher values than those from the initial solutions. The characteristic
761 behaviour of the NaOH+HW agar-based extract may be attributed to its higher purity and
762 molecular weight, promoting the formation of a stronger and stiffer network of double-helix
763 aggregates held by hydrogen bonding. The scattering intensity was further reduced when
764 holding the temperature at 95 ºC for 30 min only in the case of the commercial and the HW-
765 US agar-based samples, suggesting that structural changes continued taking place. During
766 the cooling ramp, the intensity started to increase when lowering the temperature below 35-
767 25 ºC for all the samples. This temperature range is slightly lower than the apparent gelling
768 point determined from the rheological characterization (ca. 40-35 ºC, cf. Table 1) which may
769 be due to the distinct thermal history of the samples analysed by each technique or other
770 factors such as the different sample geometry. In the case of the rheology experiments, the

771 samples were gelled directly on the rheometer plate at a cooling rate of 1 ºC/min, whereas
772 agar-based dispersions were rapidly cooled down to room temperature inside the SAXS
773 capillaries prior to the temperature ramp experiments. It is known that slow cooling leads to
774 the formation of longer helices than rapid quenching, hence promoting helix-helix
775 aggregation (Mohammed et al., 1998). Interestingly, except for the NaOH+HW sample, the
776 scattering intensity of the hydrogels after the heating and cooling ramps was lower than that
777 of the native hydrogels, suggesting that even though the agarose double-helices could re-
778 aggregate after being disrupted, they do not re-assemble in the same manner. Since the lower
779 scattering intensity after the thermal treatments is indicative of a reduced SLD contrast
780 between the agar-based hydrogel and the surrounding bulk solvent, it may be reasonable to
781 hypothesise that the double-helices re-organize to form less ordered structures, which
782 present lower physical densities or are able to hold greater amounts of water within their
783 structure. This is highly relevant from a technological perspective, since it implies that only
784 very crystalline and pure agars can maintain their structure of double-helix aggregates upon
785 heating, hence preserving their initial mechanical properties and rheological behaviour.
786

787

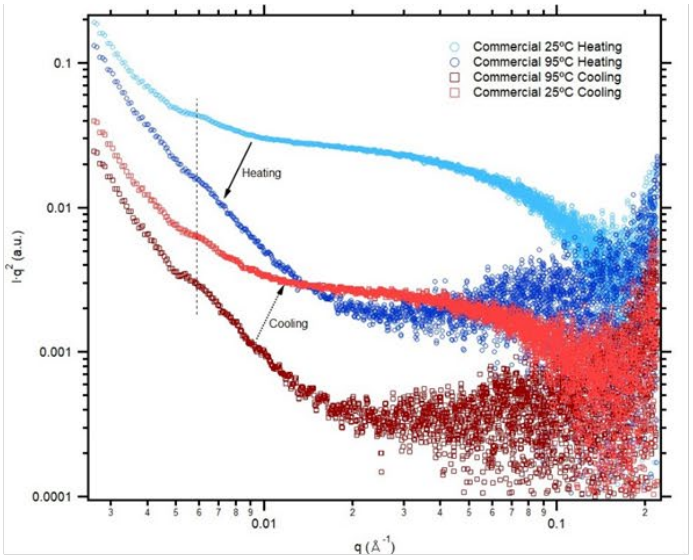
Commercial 25ºC Heating
Commercial 95ºC Heating
Commercial 95ºC Cooling
Commercial 25ºC Cooling
Heating
Cooling
I·q² (a.u.)
q (Å⁻¹)

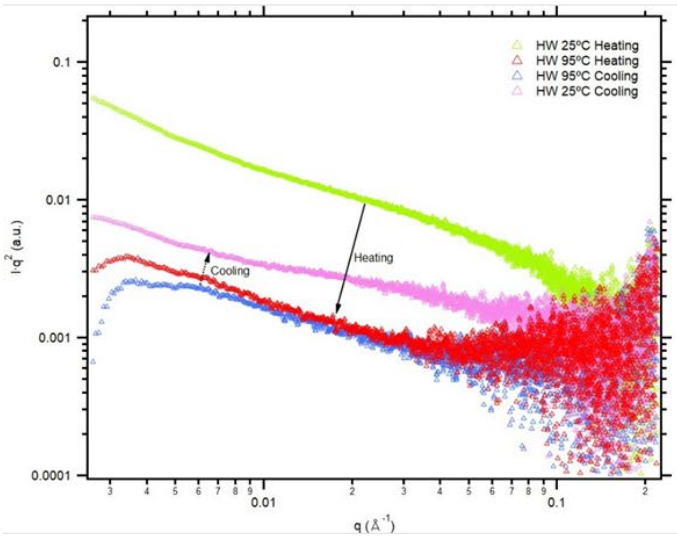
HW 25ºC Heating
HW 95ºC Heating
HW 95ºC Cooling
HW 25ºC Cooling
Heating
Cooling
I·q² (a.u.)
q (Å⁻¹)

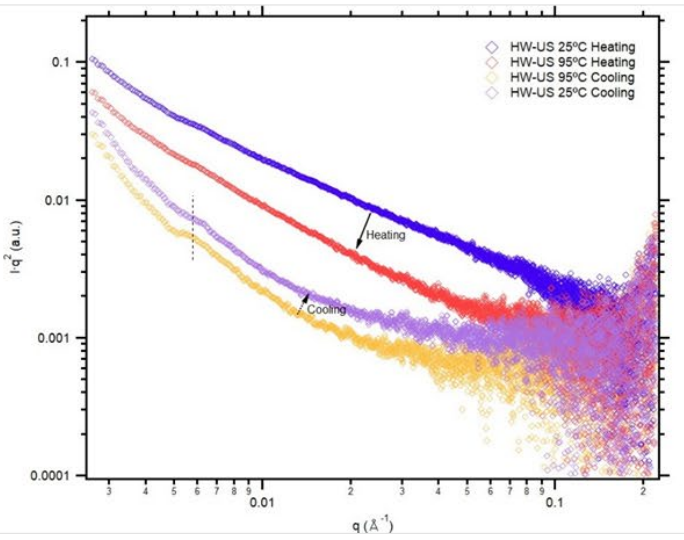
HW-US 25ºC Heating
HW-US 95ºC Heating
HW-US 95ºC Cooling
HW-US 25ºC Cooling
Heating
Cooling
I·q² (a.u.)
q (Å⁻¹)

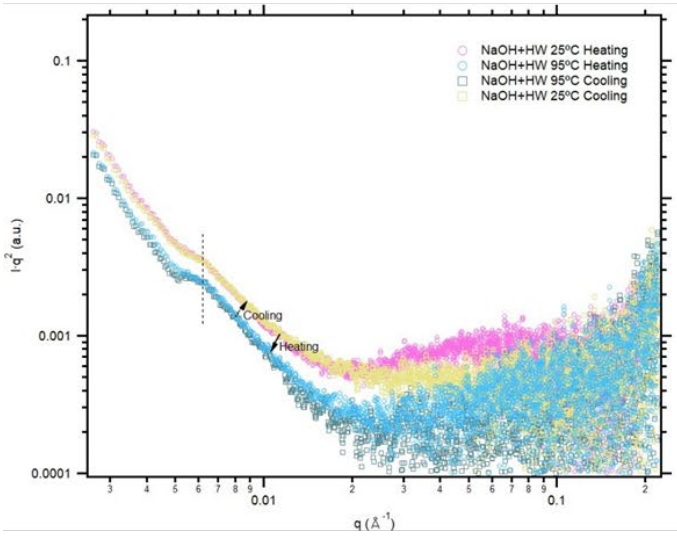
NaOH+HW 25ºC Heating
NaOH+HW 95ºC Heating
NaOH+HW 95ºC Cooling
NaOH+HW 25ºC Cooling
Cooling
Heating
I·q² (a.u.)
q (Å⁻¹)

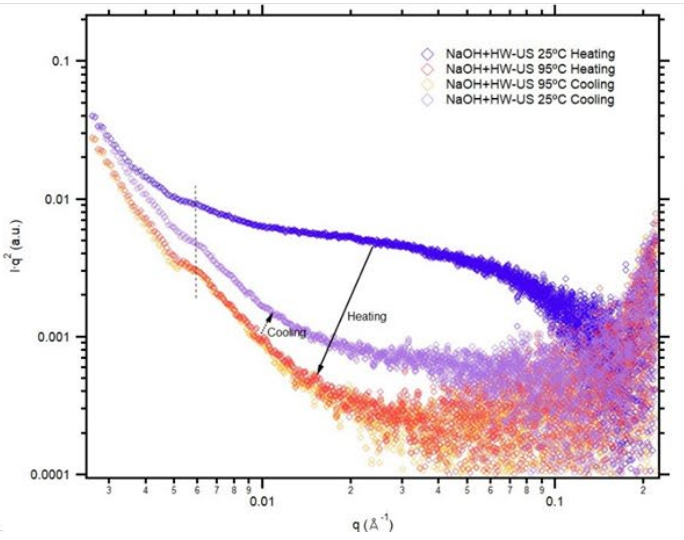
NaOH+HW-US 25ºC Heating
NaOH+HW-US 95ºC Heating
NaOH+HW-US 95ºC Cooling
NaOH+HW-US 25ºC Cooling
Heating
Cooling
I·q² (a.u.)
q (Å⁻¹)

788

Figure 5. Kratky plots from the SAXS patterns collected at 25ºC and 95ºC during the heating and cooling ramps. (A) Commercial; (B) HW; (C) HW-US; (D) NaOH+HW and (E) NaOH+HW-US.

Based on the reported results, a mechanism for the structural changes undergone by the different agar-based extracts when subjected to cooling/heating cycles is proposed in Figure 6. When the samples were initially heated to prepare aqueous dispersions, only the commercial agar showed true solution behaviour, while the agar-based extracts, due to their higher molecular weights, behaved like entangled networks, as shown by the rheological characterization. Upon cooling, the agar chains (in particular the agarose fraction) started to associate into double helices, which aggregated to form larger structures, referred to as bundles, when decreasing the temperature below 37-42 ºC. The formation of these bundles produced strong network structures and, as a result, the obtained hydrogels showed behaviour characteristic of strong gels. Surprisingly, the lower agar content in the non-purified extracts and the presence of proteins and ash did not have a strong impact on the gelation temperature. However, the mechanical performance of the obtained hydrogels was strongly influenced by the agar content, the degree of sulphation and the molecular weight of the samples. As suggested by the scattering results, a greater extent of chain association took place (i.e. thicker agarose bundles were formed) in the alkali-treated extracts, resulting in stronger and stiffer hydrogels. This may be due to the combination of their relatively high agar content, high molecular weight (compared to the commercial agar) and low sulphate content. On the contrary, the lower agarose content and higher degree of sulphation in the non-purified extracts led to the formation of smaller agarose aggregates, producing softer hydrogels. On the other hand, the presence of other components such as proteins did not

seem to impair the interconnectivity in the hydrogel network and, thus, the viscoelastic behaviour of the non-purified hydrogels was not strongly affected.

The great stability of the agarose bundles was demonstrated by the large thermal hysteresis observed for all samples in the rheology experiments. Although the scattering results show that the structure of bundles was progressively disrupted when increasing the temperature to 95 ºC, no real melting transition could be detected, suggesting that the entanglements between the agar molecular chains were not completely destroyed. The thicker agarose bundles formed in the particular case of the NaOH+HW extract, were stable even at 95 ºC, as shown by the scattering results. Interestingly, although the agarose bundles can re-associate after heating and applying a subsequent cooling cycle, it seems that less ordered structures or slightly weaker inter-chain associations were formed, indicating that unless thicker and more stable bundles are generated (such as in the case of the NaOH+HW extract), thermal treatments have an impact on the structure of the agar-based hydrogels.

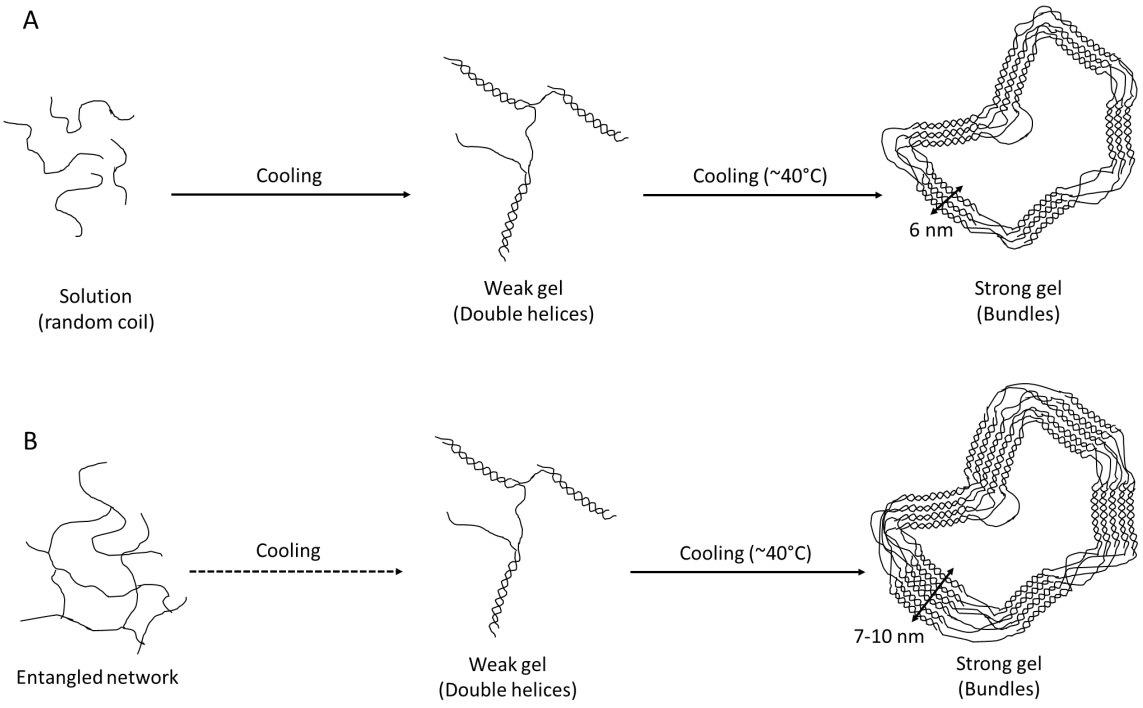

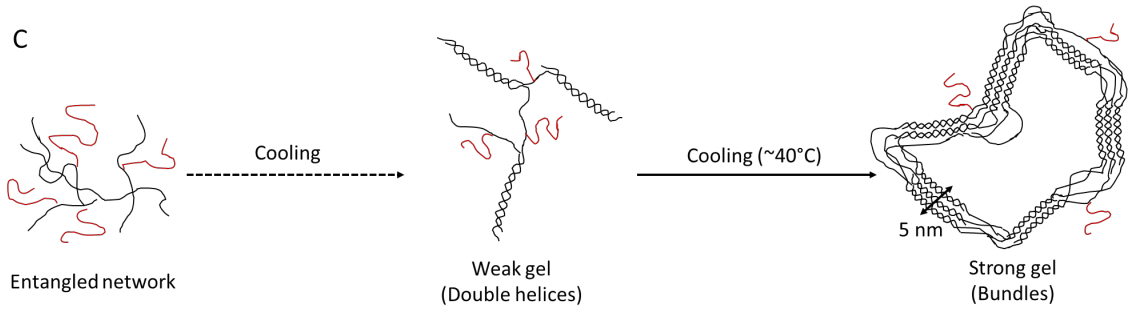

Figure 6. Scheme illustrating the proposed nanostructure of different agar-based hydrogels in their initial "solution" state and after being subjected to cooling ramps. (A) Commercial agar, (B) HW and HW-US agar-based extracts and (C) NaOH+HW and NaOH+HW-US agar-based extracts.

4. Conclusions

Agar-based extracts were produced from *Gelidium sesquipedale* using extraction protocols based on heat and combined heat-sonication treatments, with (NaOH+HW and NaOH+HW-US) and without (HW and HW-US) the application of an alkali pre-treatment. The composition of the generated extracts was strongly affected by the preparation method, the alkaline pre-treatment being critical for the subsequent extraction of more purified extracts, with higher carbohydrate contents (in particular, agar), lower sulphate contents and lower amounts of other components such as proteins. On the other hand, the harsh conditions used for the alkali pre-treatment partially degraded the agar fraction, reducing the molecular weight with respect to the non-purified extracts. With regards to the agar extraction step, the application of sonication produced extracts with lower agar contents and molecular weights.

Aqueous dispersions from the agar-based extracts underwent structural modification upon cooling due to the association of agarose chains into double helices and bundles. The temperature at which the bundles were formed was very similar for all the extracts. On the

851 other hand, the mechanical performance of the hydrogels was mostly determined by the agar
852 purity and molecular weight. Higher agar contents and molecular weights promoted a greater
853 extent of intermolecular chain association, hence producing thicker agarose bundles. This in
854 turn gave rise to the formation of stronger and stiffer hydrogels, such as those from the
855 NaOH+HW and NaOH+HW-US extracts, which were also more stable and thermally
856 resistant. The presence of non-agar components in the HW and HW-US extracts did not
857 interfere with their gelation mechanism. The lower agar content in these samples resulted in
858 the formation of softer hydrogels; however, the size of the agarose bundles was not
859 significantly affected as compared to commercial agar. As a result, the stiffness of the
860 hydrogels was similar. Although the formation of bundles is a reversible process, smaller
861 aggregates or slightly weaker structures are typically formed when subjecting the hydrogels
862 to successive heating/cooling cycles.
863
864 These results show that the gelling mechanism is essentially the same for the different agar-
865 based extracts, regardless of their composition. However, importantly, their mechanical
866 performance can be adjusted, depending on the requirements for their final application, by
867 selecting the suitable extraction protocol.
868
869 **Acknowledgements**
870 Synchrotron experiments were performed at NCD beamline at ALBA Synchrotron with the
871 collaboration of ALBA staff (2018022638 project). This work was financially supported by
872 the “Agencia Estatal de Investigación” (PCI2018-092886 Grant) and co-funded by the
873 European Union’s Horizon 2020 research and innovation programme (ERA-Net
874 SUSFOOD2). Part of this work was supported by the COST Action ES1408 European
875 network for algal-bioproducts (EUALGAE).

References

Alehosseini, A., del Pulgar, E.-M. G., Gómez-Mascaraque, L. G., Martínez-Sanz, M., Fabra, M. J., Sanz, Y., . . . Lopez-Rubio, A. (2018). Unpurified *Gelidium*-extracted carbohydrate-rich fractions improve probiotic protection during storage. *LWT,* 96, 694-703.

Araki, C. (1966). Some recent studies on the polysaccharides of agarophytes. *Proceedings of the Fifth International Seaweed Symposium, Halifax, August 25–28, 1965* (pp. 3-17): Elsevier.

Armisen, R., & Galatas, F. (1987). Production, properties and uses of agar. *Production and utilization of products from commercial seaweeds. FAO Fish. Tech. Pap,* 288, 1-57.

Arnold, O., Bilheux, J. C., Borreguero, J. M., Buts, A., Campbell, S. I., Chapon, L., . . . Zikovsky, J. (2014). Mantid—Data analysis and visualization package for neutron scattering and μ SR experiments. *Nuclear Instruments and Methods in Physics Research Section A: Accelerators, Spectrometers, Detectors and Associated Equipment,* 764, 156-166.

Arnott, S., Fulmer, A., Scott, W. E., Dea, I. C. M., Moorhouse, R., & Rees, D. A. (1974). The agarose double helix and its function in agarose gel structure. *Journal of Molecular Biology,* 90(2), 269-284.

Aymard, P., Martin, D. R., Plucknett, K., Foster, T. J., Clark, A. H., & Norton, I. T. (2001). Influence of thermal history on the structural and mechanical properties of agarose gels. *Biopolymers,* 59(3), 131-144.

Bellion, C., Brigand, G., Prome, J.-C., Welti, D., & Bociek, S. (1983). Identification et caractérisation des précurseurs biologiques des carraghénanes par spectroscopie de RMN-13C. *Carbohydrate Research,* 119, 31-48.

Carmona, R., Vergara, J. J., Lahaye, M., & Niell, F. X. (1998). Light quality affects morphology and polysaccharide yield and composition of Gelidium sesquipedale (Rhodophyceae). *Journal of Applied Phycology,* 10(3), 323.

Chizhov, O., Zolotarev, B., Usov, A., Rechter, M., & Kocchetkov, N. (1971). Mass-spectrometric characterization of 3, 6-anhydro-galactose derivatives. *Carbohydrate Research,* 16(1), 29-38.

Dai, B., & Matsukawa, S. (2012). NMR studies of the gelation mechanism and molecular dynamics in agar solutions. *Food Hydrocolloids,* 26(1), 181-186.

Djabourov, M., Clark, A. H., Rowlands, D. W., & Ross-Murphy, S. B. (1989). Small-angle x-ray scattering characterization of agarose sols and gels. *Macromolecules,* 22(1), 180-188.

Duckworth, M., & Yaphe, W. (1971). The structure of agar: Part I. Fractionation of a complex mixture of polysaccharides. *Carbohydrate Research,* 16(1), 189-197.

Fatin-Rouge, N., Wilkinson, K. J., & Buffle, J. (2006). Combining small angle neutron scattering (SANS) and fluorescence correlation spectroscopy (FCS) measurements to relate diffusion in agarose gels to structure. *The Journal of Physical Chemistry B,* 110(41), 20133-20142.

Fernández, E., López, D., Mijangos, C., Duskova-Smrckova, M., Ilavsky, M., & Dusek, K. (2008). Rheological and thermal properties of agarose aqueous solutions and hydrogels. *Journal of Polymer Science Part B: Polymer Physics,* 46(3), 322-328.

Freile-Pelegrín, Y., & Robledo, D. (1997). Influence of alkali treatment on agar from Gracilaria cornea from Yucatán, México. *Journal of Applied Phycology,* 9(6), 533.

Gómez-Mascaraque, L. G., Llavata-Cabrero, B., Martínez-Sanz, M., Fabra, M. J., & López-Rubio, A. (2018). Self-assembled gelatin-ι-carrageenan encapsulation structures for intestinal-targeted release applications. *Journal of Colloid and Interface Science,* 517, 113-123.

Indovina, P., Tettamanti, E., Micciancio-Giammarinaro, M., & Palma, M. (1979). Thermal hysteresis and reversibility of gel–sol transition in agarose–water systemsa). *The Journal of Chemical Physics,* 70(6), 2841-2847.

Knutsen, S., Myslabodski, D., Larsen, B., & Usov, A. (1994). A modified system of nomenclature for red algal galactans. *Botanica Marina,* 37(2), 163-170.

Krueger, S., Andrews, A. P., & Nossal, R. (1994). Small angle neutron scattering studies of structural characteristics of agarose gels. *Biophysical chemistry,* 53(1-2), 85-94.

Kumar, V., & Fotedar, R. (2009). Agar extraction process for Gracilaria cliftonii (Withell, Millar, & Kraft, 1994). *Carbohydrate Polymers,* 78(4), 813-819.

Lahrech, K., Safouane, A., & Peyrellasse, J. (2005). Sol state formation and melting of agar gels rheological study. *Physica A: Statistical Mechanics and its Applications,* 358(1), 205-211.

Lee, W.-K., Lim, Y.-Y., Leow, A. T.-C., Namasivayam, P., Abdullah, J. O., & Ho, C.-L. (2017). Factors affecting yield and gelling properties of agar. *Journal of Applied Phycology,* 29(3), 1527-1540.

Lopez-Sanchez, P., Martinez-Sanz, M., Bonilla, M. R., Wang, D., Gilbert, E. P., Stokes, J. R., & Gidley, M. J. (2017). Cellulose-pectin composite hydrogels: Intermolecular interactions and material properties depend on order of assembly. *Carbohydrate Polymers,* 162, 71-81.

Martínez-Sanz, M., Gidley, M. J., & Gilbert, E. P. (2016). Hierarchical architecture of bacterial cellulose and composite plant cell wall polysaccharide hydrogels using small angle neutron scattering. *Soft Matter,* 12(5), 1534-1549.

Martínez-Sanz, M., Gómez-Mascaraque, L. G., Ballester, A. R., Martínez-Abad, A., Brodkorb, A., & López-Rubio, A. (2019). Production of unpurified agar-based extracts from red seaweed Gelidium sesquipedale by means of simplified extraction protocols. *Algal Research,* 38, 101420.

Martínez-Sanz, M., Martínez-Abad, A., & López-Rubio, A. (2019). Cost-efficient bio-based food packaging films from unpurified agar-based extracts. *Food Packaging and Shelf Life,* 21, 100367.

Martínez-Sanz, M., Mikkelsen, D., Flanagan, B., Gidley, M. J., & Gilbert, E. P. (2016). Multi-scale model for the hierarchical architecture of native cellulose hydrogels. *Carbohydrate Polymers,* 147, 542-555.

Matsuhiro, B., & Urzúa, C. (1990). Agars from Gelidium rex (Gelidiales, Rhodophyta). *Thirteenth International Seaweed Symposium* (pp. 545-549): Springer.

Medina-Esquivel, R., Freile-Pelegrin, Y., Quintana-Owen, P., Yáñez-Limón, J., & Alvarado-Gil, J. (2008). Measurement of the sol–gel transition temperature in agar. *International Journal of Thermophysics,* 29(6), 2036.

Meena, R., Prasad, K., Ganesan, M., & Siddhanta, A. K. (2007). Superior quality agar from Gracilaria species (Gracilariales, Rhodophyta) collected from the Gulf of Mannar, India. *Journal of Applied Phycology,* 20(4), 397.

971 Melo, M., Feitosa, J., Freitas, A., & De Paula, R. (2002). Isolation and characterization
972 of soluble sulfated polysaccharide from the red seaweed Gracilaria cornea.
973 *Carbohydrate Polymers,* 49(4), 491-498.
974 Millán, A. J., Moreno, R., & Nieto, M. a. I. (2002). Thermogelling polysaccharides for
975 aqueous gelcasting—part I: a comparative study of gelling additives. *Journal of*
976 *the European Ceramic Society,* 22(13), 2209-2215.
977 Mohammed, Z. H., Hember, M. W. N., Richardson, R. K., & Morris, E. R. (1998).
978 Kinetic and equilibrium processes in the formation and melting of agarose gels.
979 *Carbohydrate Polymers,* 36(1), 15-26.
980 Mouradi-Givernaud, A., Givernaud, T., Morvan, H., & Cosson, J. (1992). Agar from
981 Gelidium latifolium (Rhodophyceae, Gelidiales): biochemical composition and
982 seasonal variations. *Botanica Marina,* 35(2), 153-160.
983 Mouradi-Givernaud, A., Hassani, L. A., Givernaud, T., Lemoine, Y., & Benharbet, O.
984 (1999). Biology and agar composition of Gelidium sesquipedale harvested along
985 the Atlantic coast of Morocco. *Hydrobiologia,* 398, 391-395.
986 Murano, E., Toffanin, R., Zanetti, F., Knutsen, S., Paoletti, S., & Rizzo, R. (1992).
987 Chemical and macromolecular characterisation of agar polymers from Gracilaria
988 dura (C. Agardh) J. Agardh (Gracilariaceae, Rhodophyta). *Carbohydrate*
989 *Polymers,* 18(3), 171-178.
990 Nakauma, M., Ishihara, S., Funami, T., Yamamoto, T., & Higashimori, M. (2014).
991 Deformation behavior of agar gel on a soft substrate during instrumental
992 compression and its computer simulation. *Food Hydrocolloids,* 36, 301-307.
993 Nordqvist, D., & Vilgis, T. A. (2011). Rheological Study of the Gelation Process of
994 Agarose-Based Solutions. *Food Biophysics,* 6(4), 450.
995 Quemener, B., & Lahaye, M. (1998). Comparative analysis of sulfated galactans from
996 red algae by reductive hydrolysis and mild methanolysis coupled to two
997 different HPLC techniques. *Journal of Applied Phycology,* 10(1), 75.
998 Ramzi, M., Rochas, C., & Guenet, J.-M. (2000). On the occurrence of ternary
999 complexes in agarose gels as studied by the contrast variation method.
1000 *International Journal of Biological Macromolecules,* 27(2), 163-170.
1001 Rochas, C., Hecht, A. M., & Geissler, E. (1999). Scattering properties of agarose gels.
1002 *Macromolecular Symposia* (Vol. 138, pp. 157-163): Wiley Online Library.
1003 Rochas, C., & Lahaye, M. (1989). Average molecular weight and molecular weight
1004 distribution of agarose and agarose-type polysaccharides. *Carbohydrate*
1005 *Polymers,* 10(4), 289-298.
1006 Ross, K., Pyrak-Nolte, L., & Campanella, O. (2006). The effect of mixing conditions on
1007 the material properties of an agar gel—microstructural and macrostructural
1008 considerations. *Food Hydrocolloids,* 20(1), 79-87.
1009 Russ, N., Zielbauer, B. I., Koynov, K., & Vilgis, T. A. (2013). Influence of Nongelling
1010 Hydrocolloids on the Gelation of Agarose. *Biomacromolecules,* 14(11), 4116-
1011 4124.
1012 Santinath Singh, S., Aswal, V. K., & Bohidar, H. B. (2011). Internal structures of agar-
1013 gelatin co-hydrogels by light scattering, small-angle neutron scattering and
1014 rheology. *The European Physical Journal E,* 34(6), 62.
1015 Sharma, S., & Bhattacharya, S. (2014). Strain and strain rate dependence of gellan, agar
1016 and agar–gellan gels as model systems. *Journal of Food Engineering,* 141, 93-
1017 98.
1018 Singh, S. S., Aswal, V., & Bohidar, H. (2007). Structural studies of agar–gelatin
1019 complex coacervates by small angle neutron scattering, rheology and differential

scanning calorimetry. *International Journal of Biological Macromolecules,* 41(3), 301-307.

Singh, S. S., Aswal, V., & Bohidar, H. (2009). Structural evolution of aging agar-gelatin co-hydrogels. *Polymer,* 50(23), 5589-5597.

Sokolova, A., Whitten, A. E., de Campo, L., Christoforidis, J., Eltobaji, A., Barnes, J., . . . Berry, A. (2019). Performance and characteristics of the BILBY time-of-flight small-angle neutron scattering instrument. *Journal of Applied Crystallography,* 52(1).

Sousa, A. M., Borges, J., Silva, A. F., & Gonçalves, M. P. (2013). Influence of the extraction process on the rheological and structural properties of agars. *Carbohydrate Polymers,* 96(1), 163-171.

Sousa, A. M., Morais, S., Abreu, M. H., Pereira, R., Sousa-Pinto, I., Cabrita, E. J., . . . Gonçalves, M. P. (2012). Structural, physical, and chemical modifications induced by microwave heating on native agar-like galactans. *Journal of Agricultural and Food Chemistry,* 60(19), 4977-4985.

Stevenson, T. T., & Furneaux, R. H. (1991). Chemical methods for the analysis of sulphated galactans from red algae. *Carbohydrate Research,* 210, 277-298.

Trefna, H. D., & Ström, A. (2019). Hydrogels as a water bolus during hyperthermia treatment. *Physics in Medicine & Biology*.

Yang, Z., Hemar, Y., Hilliou, L., Gilbert, E. P., McGillivray, D. J., Williams, M. A. K., & Chaieb, S. (2016). Nonlinear Behavior of Gelatin Networks Reveals a Hierarchical Structure. *Biomacromolecules,* 17(2), 590-600.

Yousefi, M. K., Islami, H. R., & Filizadeh, Y. (2013). Effect of extraction process on agar properties of Gracilaria corticata (Rhodophyta) collected from the Persian Gulf. *Phycologia,* 52(6), 481-487.

Yu, L., Yakubov, G. E., Martínez-Sanz, M., Gilbert, E. P., & Stokes, J. R. (2018). Rheological and structural properties of complex arabinoxylans from Plantago ovata seed mucilage under non-gelled conditions. *Carbohydrate Polymers,* 193, 179-188.

Supplementary Material

Table S1. Elemental composition of the agar-based extracts (% dry weight).

	N (%)	**C (%)**	**S (%)**
Commercial	0.24	43.30	0.70
HW	1.82	27.70	3.27
HW-US	1.69	31.20	2.22
NaOH+HW	0.64	41.90	0.63
NaOH+HW-US	1.17	38.30	0.65

Table S2. Neutron and X-ray scattering length densities for native agarose ($C_{12}H_{18}O_9$) and after H/D exchange of the labille hydroxyl groups ($C_{12}H_{14}D_4O_9$). The agarose physical density was taken as $\rho_{agarose}$ = 1.7 g/cm^3 (Rochas et al., 1999).

	Neutron SLD (10^{10} cm^{-2})	X-ray SLD (10^{10} cm^{-2})
Agarose	2.16	15.32
Agarose (D_2O exchanged)	3.51	15.13
H_2O	-0.56	9.47
D_2O	6.38	9.37

Table S3. Parameters obtained from fits of the unified model for the commercial agar gel. Standard deviations on the last digit are shown in parentheses.

	H_2O SAXS	SANS				
		H_2O	20%D_2O	35%D_2O	60%D_2O	D_2O
B_1 (cm^{-1}·sr^{-1}·Å^{-P1})	0.0018 (3)	0.0006 (3)	0.0004 (4)	0.00005 (2)	0.00005 (2)	0.00067 (2)
P_1	2.611 (4)	1.91 (1)	1.82 (2)	1.9 (1)	1.9 (1)	1.89 (1)
G_2 (cm^{-1}·sr^{-1})	47.2 (5)	0.46 (1)	0.12 (2)	0.03 (1)	0.03 (1)	0.54 (1)
R_{g2} (nm)	5.63 (2)					
B_2 (cm^{-1}·sr^{-1}·Å^{-P2})	0.0001 (1)	0.0064 (3)	0.003 (1)	0.001 (1)	0.00001 (1)	0.00001 (1)
P_2	3.85 (1)	1.0 (2)	1.0 (1)	1.0 (2)	1.0 (5)	4.0 (1)

Table S4. Parameters obtained from fits of the unified model for the HW agar-based gel. Standard deviations on the last digit are shown in parentheses.

	H_2O SAXS	SANS				
		H_2O	20%D_2O	35%D_2O	60%D_2O	D_2O

B_1 ($cm^{-1}\cdot sr^{-1}\cdot Å^{-P1}$)	0.00065 (1)	0.00003 (1)	0.00001 (1)	0.00001 (1)	0.00001 (1)	0.00001 (2)
P_1	2.709 (2)	2.66 (1)	2.517 (1)	2.74 (6)	2.52 (4)	2.39 (1)
G_2 ($cm^{-1}\cdot sr^{-1}$)	10.3 (1)	0.39 (1)	0.065 (3)	0.02 (1)	0.05 (1)	0.35 (1)
R_{g2} (nm)	4.95 (2)					
B_2 ($cm^{-1}\cdot sr^{-1}\cdot Å^{-P2}$)	0.00003 (1)	0.0018 (1)	0.0018 (1)	0.0001 (4)	0.0004 (1)	0.00001 (1)
P_2	4.0 (1)	1.0 (3)	1.00 (1)	1.6 (5)	1.0 (7)	3.7 (2)

Table S5. Parameters obtained from fits of the unified model for the HW-US agar-based gel. Standard deviations on the last digit are shown in parentheses.

	H_2O SAXS	SANS				
		H_2O	20%D_2O	35%D_2O	60%D_2O	D_2O
B_1 ($cm^{-1}\cdot sr^{-1}\cdot Å^{-P1}$)	0.00024 (1)	0.00003 (1)	0.00002 (1)	0.00002 (1)	0.00003 (1)	0.00013 (1)
P_1	2.97 (1)	2.54 (1)	2.39 (3)	2.28 (4)	2.55 (5)	2.25 (1)
G_2 ($cm^{-1}\cdot sr^{-1}$)	6.7 (1)	0.35 (1)	0.08 (1)	0.01 (1)	0.05 (1)	0.33 (1)
R_{g2} (nm)	4.59 (3)					
B_2 ($cm^{-1}\cdot sr^{-1}\cdot Å^{-P2}$)	0.00002 (1)	0.00001 (4)	0.0025 (1)	0.001 (1)	0.00001 (1)	0.00001 (1)
P_2	3.97 (1)	3.7 (4)	1.0 (2)	1.0 (4)	1.7 (7)	4.0 (2)

Table S6. Parameters obtained from fits of the unified model for the NaOH+HW agar-based gel. Standard deviations on the last digit are shown in parentheses.

	H_2O SAXS	SANS				
		H_2O	20%D_2O	35%D_2O	60%D_2O	D_2O
B_1 ($cm^{-1}\cdot sr^{-1}\cdot Å^{-P1}$)	0.0000002 (1)	0.00004 (1)	0.00003 (1)	0.000002 (2)	0.000001 (1)	0.00005 (1)
P_1	3.92 (1)	2.47 (1)	2.29 (6)	2.6 (1)	2.78 (8)	2.45 (2)
G_2 ($cm^{-1}\cdot sr^{-1}$)	2.63 (1)	2.46 (2)	0.67 (4)	0.14 (2)	0.22 (1)	3.07 (4)

R_{g2} (nm)	9.58 (3)					
B_2 ($cm^{-1}\cdot sr^{-1}\cdot Å^{-P2}$)	0.00018 (1)	0.0066 (1)	0.0009 (3)	0.001 (1)	0.00068 (3)	0.00001 (1)
P_2	2.50 (1)	1.11 (1)	1.4 (1)	1.0 (2)	1.1 (2)	2.93 (2)

Table S7. Parameters obtained from fits of the unified model for the NaOH+HW-US agar-based gel. Standard deviations on the last digit are shown in parentheses.

	H_2O SAXS	SANS				
		H_2O	20%D_2O	35%D_2O	60%D_2O	D_2O
B_1 ($cm^{-1}\cdot sr^{-1}\cdot Å^{-P1}$)	0.0002 (1)	0.00019 (1)	0.00019 (5)	0.000001 (6)	0.000001 (2)	0.00010 (1)
P_1	2.745 (3)	2.16 (1)	1.91 (5)	2.7 (1)	2.87 (5)	2.34 (2)
G_2 ($cm^{-1}\cdot sr^{-1}$)	14.1 (1)	0.74 (1)	0.15 (3)	0.03 (1)	0.09 (1)	1.10 (2)
R_{g2} (nm)	6.67 (3)					
B_2 ($cm^{-1}\cdot sr^{-1}\cdot Å^{-P2}$)	0.00004 (1)	0.000001 (5)	0.003 (1)	0.001 (1)	0.0003 (1)	0.000001 (1)
P_2	3.56 (1)	4.0 (2)	1.0 (1)	1.0 (2)	1.2 (4)	3.33 (6)

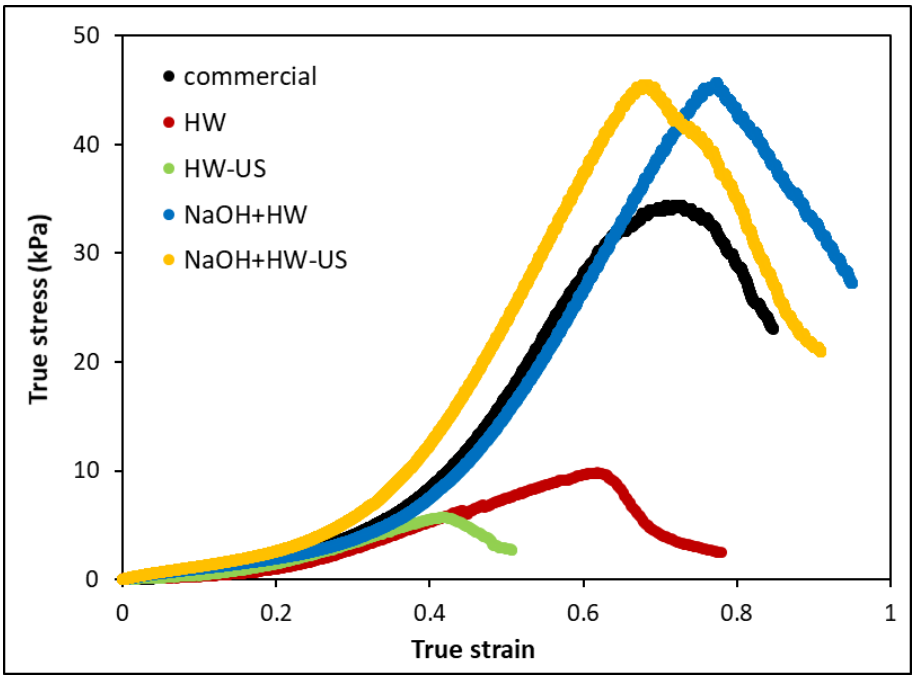

Figure S1. Representative compressive true stress-true strain curves for the agar-based hydrogels.

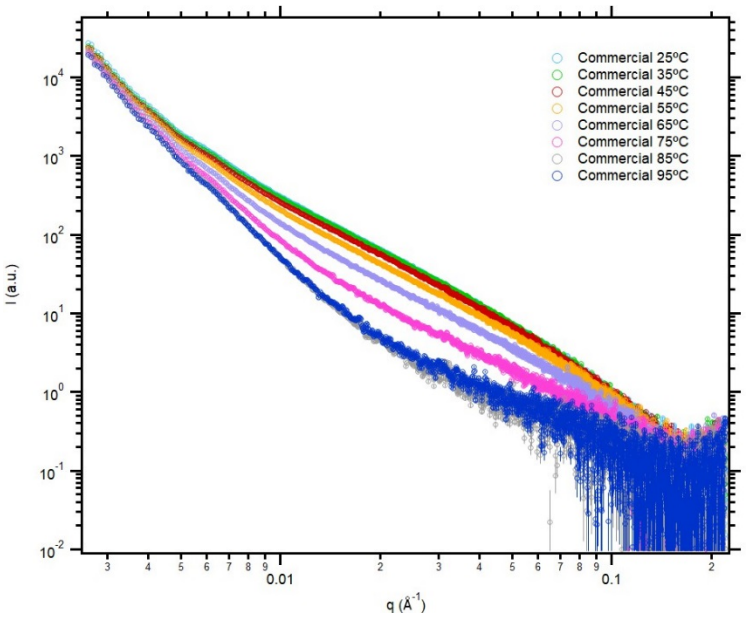

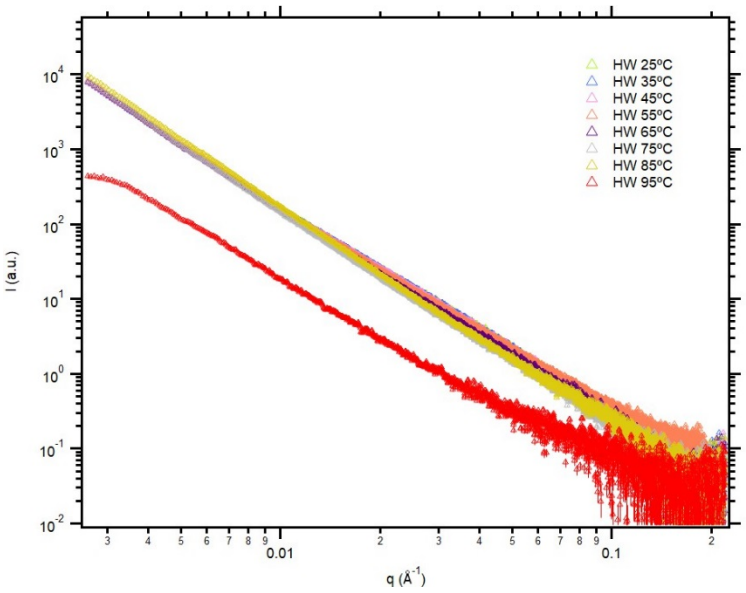

1077

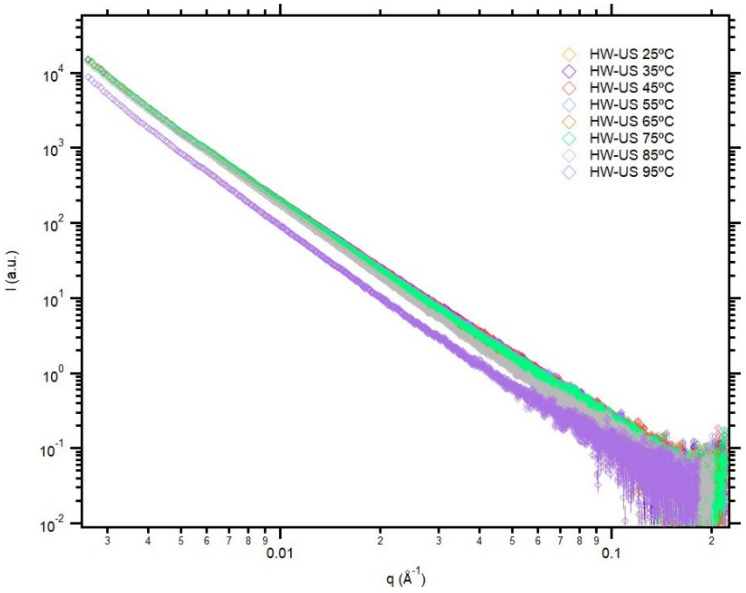

1078

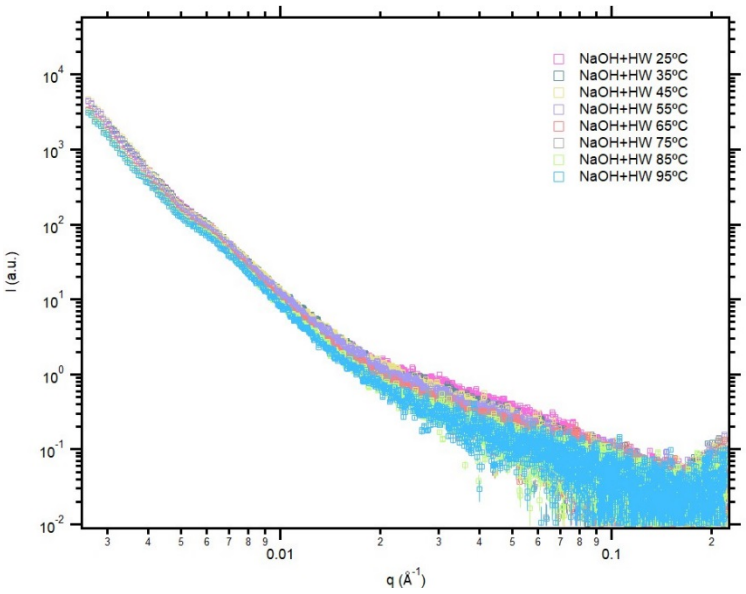

1079

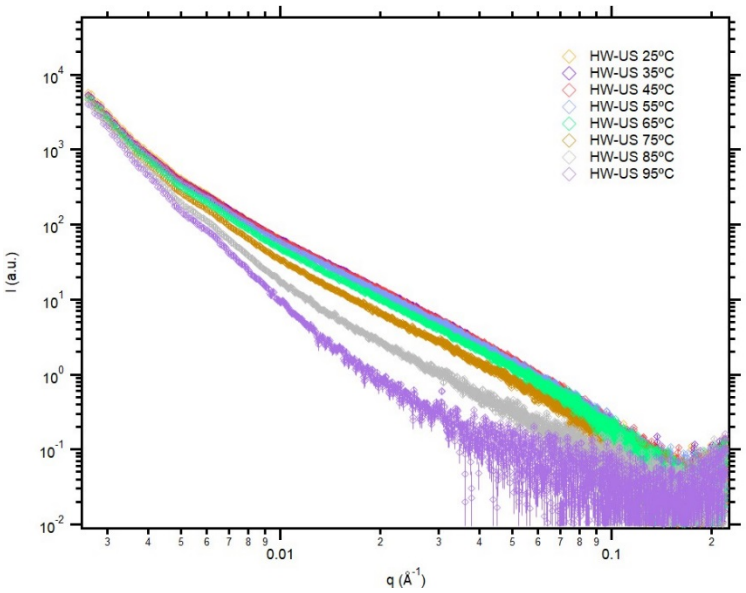

1080

1081 **Figure S2.** SAXS patterns from the heating ramps (25-95ºC) of agar-based extracts: (A)

1082 Commercial; (B) HW; (C) HW-US; (D) NaOH+HW and (E) NaOH+HW-US.

1083

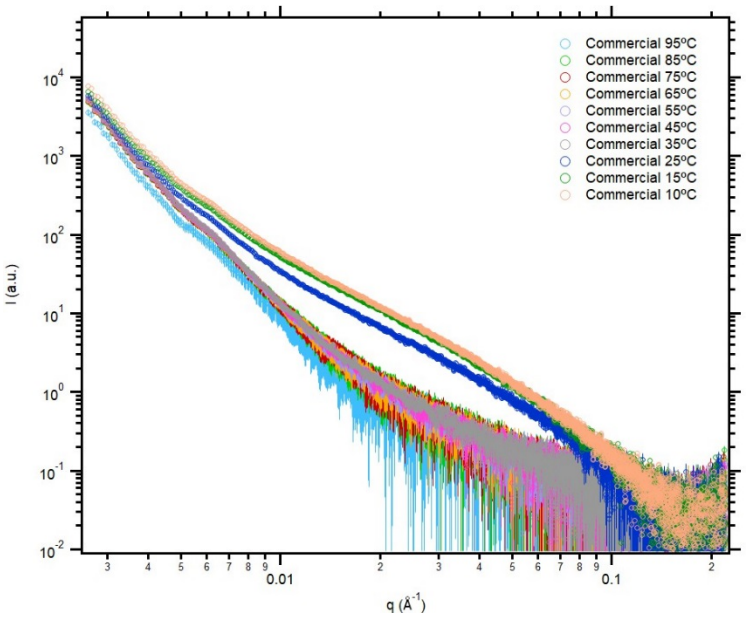

1084

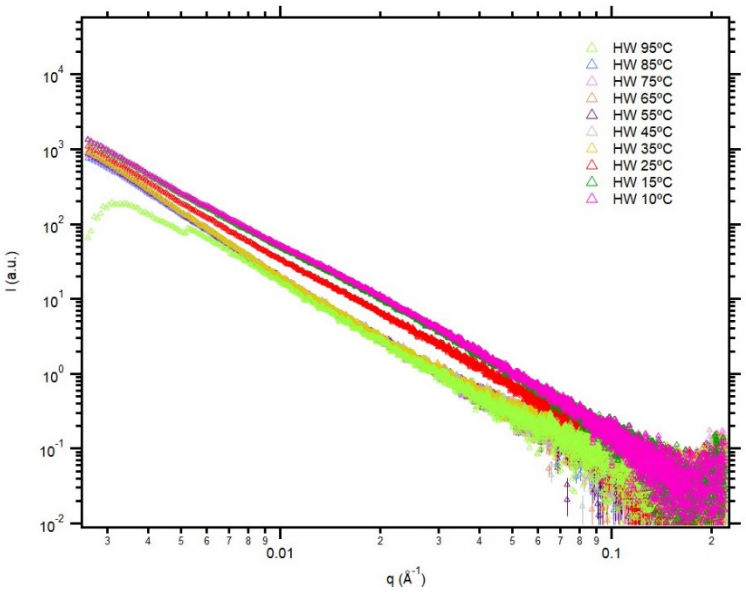

1085

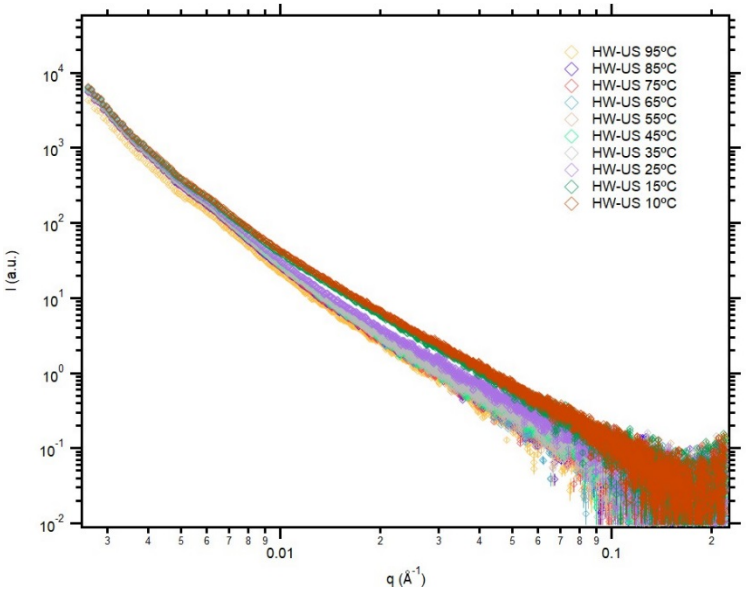

1086

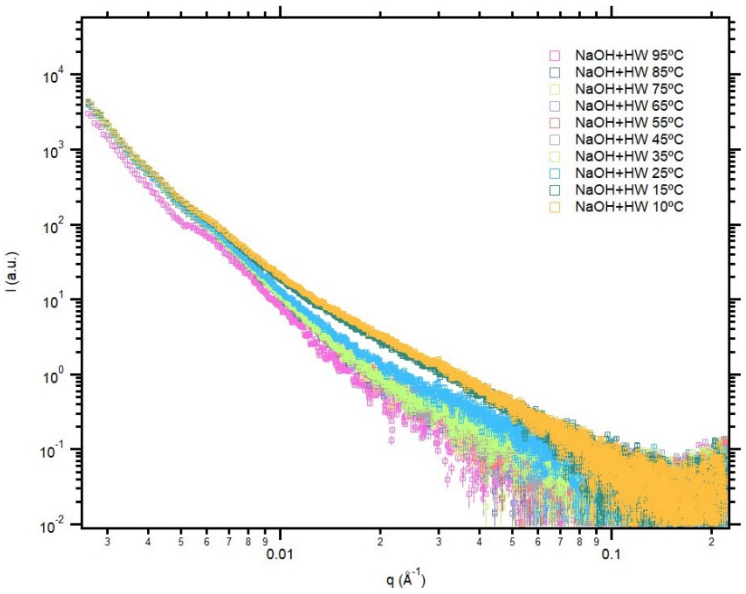

1087

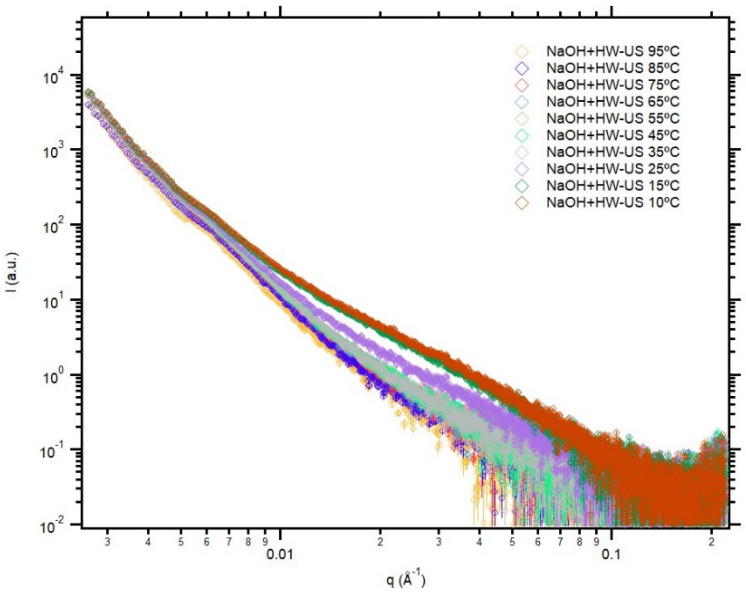

1088

1089 **Figure S3.** SAXS patterns from the cooling ramps (95-10ºC) of agar-based extracts: (A)

1090 Commercial; (B) HW; (C) HW-US; (D) NaOH+HW and (E) NaOH+HW-US.